This is the peer-reviewed, final accepted version for American Mineralogist, published by the Mineralogical Society of America.
The published version is subject to change. Cite as Authors (Year) Title. American Mineralogist, in press.
DOI: https://doi.org/10.2138/am-2020-7395. http://www.minsocam.org/

REVISION 2

Titanium diffusion profiles and melt inclusion chemistry and morphology in quartz from the Tshirege Member of the Bandelier Tuff

JOSEPH R. BORO[1], JOHN A. WOLFF[1], OWEN K. NEILL[2], ARRON R. STEINER[1], AND FRANK C. RAMOS[3]

[1]School of the Environment, Washington State University, Pullman, WA 99163, USA

[2]School of Earth and Environmental Sciences, University of Michigan, Ann Arbor, MI 48109, USA

[3]Department of Geological Sciences, New Mexico State University, Las Cruces, NM 88003, USA

Keywords: caldera, cathodoluminescence, diffusion, inclusion, melt, quartz, tuff, volcano

ABSTRACT

Many rhyolites contain quartz crystals with relatively Ti-rich rims and Ti-poor cores, with a sharp interface between zones, attributed to partial dissolution followed by overgrowth following a heating event due to mafic recharge of the system. Quartz crystals in the compositionally zoned, high-silica rhyolite Tshirege Member of the Bandelier Tuff, erupted at 1.26 Ma from the Valles caldera, New Mexico, show a range in zoning styles with Ti-rich rims becoming more abundant upwards in the ignimbrite sheet among progressively less evolved magma compositions. Here we compare times between quartz overgrowth and eruption obtained by applying Ti diffusion coefficients to Ti concentration profiles in Tshirege Member quartz crystals with those from cathodoluminescence (CL) brightness profiles, and show that panchromatic CL provides only a crude proxy for Ti in quartz in this unit. Titanium concentrations are measured to detection limits of ~1.2 ppm with small analytical errors (<5%)

Always consult and cite the final, published document. See http:/www.minsocam.org or GeoscienceWorld

This is the peer-reviewed, final accepted version for American Mineralogist, published by the Mineralogical Society of America.
The published version is subject to change. Cite as Authors (Year) Title. American Mineralogist, in press.
DOI: https://doi.org/10.2138/am-2020-7395. http://www.minsocam.org/

using MAN backgrounds, blank corrections, and oblique corrected transects to resolve diffusion-relaxed zone boundaries as thin as ~10 μm. Timescales derived from Ti profiles using the widely applied Ti-in-quartz diffusion coefficients of Cherniak et al. (2007) range from 60 to 10,000 years, suggesting heating and mobilization events at different times prior to the eruption. However, use of the newer Ti diffusivities reported by Jollands et al. (2020) yields timescales up to three orders of magnitude longer, including results that are geologically unreasonable for the Bandelier system. We suggest that assumptions commonly made in diffusion modeling, specifically about the form of the Ti zoning profile prior to diffusive relaxation, may be invalid.

Melt inclusions in the Ti-poor cores of late-erupted quartz are chemically akin to early erupted melt compositions, while adhering and groundmass glasses more closely reflect the composition of the host pumice. Heating and mobilization events identified from quartz Ti zoning are thus linked to overall compositional zoning of the tuff, which may have been produced by repeated episodes of melting of a crystal cumulate cognate to the early-erupted, evolved rhyolite. Quartz-hosted melt inclusion faceting suggests the development of a crystal mush over a minimum time frame of 1,000 – 10,000 years prior to recharge events that produced the eruptible Tshirege magma.

INTRODUCTION

Diffusion modeling of element concentration profiles in crystals is a fruitful way of extracting timescales of processes occurring at elevated temperatures in geologic systems. The approach relies on some assumptions, such as starting conditions for the diffusion episode and that the concentration profiles being modeled are indeed the result of ionic diffusion. In studies of volcanic systems, diffusion profiles can help determine residence times of crystals in magma

Always consult and cite the final, published document. See http:/www.minsocam.org or GeoscienceWorld

This is the peer-reviewed, final accepted version for American Mineralogist, published by the Mineralogical Society of America.
The published version is subject to change. Cite as Authors (Year) Title. American Mineralogist, in press.
DOI: https://doi.org/10.2138/am-2020-7395. http://www.minsocam.org/

based on compositional zoning of the minerals of interest. Diffusion modeling can also be used to determine the time elapsed between an identifiable event in the history of a crystal (e.g., overgrowth on a resorption surface) and eruption (Costa and Dungan, 2005; Morgan and Blake, 2006; Wark et al., 2007; Costa et al., 2008; Till et al., 2015). Timescales deduced from the diffusive blurring of an overgrowth boundary can provide insights on how magma systems respond to disturbance, such as rejuvenation and heating by magmatic recharge, shortly before an eruption. This approach has yielded estimates of short activation timescales (<1 year – 1000 years) preceding past catastrophic silicic caldera-forming 'super-eruptions' (Wark et al., 2007; Matthews et al., 2012; Till et al., 2015; Gualda and Sutton, 2016; Cooper et al., 2017). Smaller, much more frequent eruptions may also have activation timescales of < 1 year, for example Calbuco volcano, 2015 (Arzilli et al., 2019).

In rhyolitic volcanic systems, quartz is an attractive and widely-used target for diffusion modeling because quartz crystals are usually large and of effectively constant major element composition. Trace element substitutions, particularly that of Ti^{4+} for tetrahedral Si^{4+} in the quartz structure (Götze, 2012; Leeman et al., 2012), result in enhanced cathodoluminescence (CL) brightness that in principle allows easy identification of trace cation concentration zoning, and because the behavior of Ti in quartz is well-studied. Peppard et al. (2001) provided the first detailed description of CL zoning in quartz from a high-silica rhyolite (the Bishop Tuff). Wark and Watson (2006) calibrated Ti-in-quartz as a geothermometer, while Cherniak et al. (2007) reported results for the diffusion coefficient of Ti (D_{Ti}) in quartz. These studies spawned a significant literature linking Ti-in-quartz variations, CL zoning, and magmatic temperature to estimates of crystal residence timescales and the rejuvenation of large stagnant silicic magma bodies to an eruptible state, as well as new calibrations of the Ti-in-quartz (TitaniQ) thermometer

Always consult and cite the final, published document. See http:/www.minsocam.org or GeoscienceWorld

This is the peer-reviewed, final accepted version for American Mineralogist, published by the Mineralogical Society of America.
The published version is subject to change. Cite as Authors (Year) Title. American Mineralogist, in press.
DOI: https://doi.org/10.2138/am-2020-7395. http://www.minsocam.org/

(Hayden and Watson, 2007; Wark et al., 2007; Shane et al., 2008; Campbell et al., 2009; Thomas et al., 2010; Gualda et al., 2012; Huang and Audétat, 2012; Matthews et al., 2012; Thomas and Watson, 2012; Wilson et al., 2012; Wilcock et al., 2013; Gualda and Sutton, 2016; Pamukcu et al., 2015; Seitz et al., 2016; Cooper et al., 2017). The temperature sensitivity of D_{Ti} requires accurate knowledge of temperature during the diffusion episode in order to extract timescales from modeled diffusion profiles, placing demands on geothermometry. Also, the application of the Ti-in-quartz geothermometer requires precise knowledge of the activity of Ti in the melt in equilibrium with the quartz, a parameter which is not always well constrained (Huang and Audétat, 2012; Matthews et al., 2012; Thomas and Watson, 2012; Wilson et al., 2012).

Much of the interest in using Ti-in-quartz diffusion to estimate silicic magma rejuvenation timescales stems from the geologically short durations that result from applying the diffusivities of Cherniak et al. (2007) to observed Ti zoning profiles, with implications for eruption prediction in regions of silicic volcanism. The estimated durations rely on the assumption of an initial step-function zone boundary separating quartz interiors from rims grown following a heating and resorption event (Wark et al., 2007), and range from hundreds of years down to less than a year (Wark et al., 2007; Gualda et al., 2012; Wilcock et al., 2013; Seitz et al., 2016; Gualda and Sutton, 2016). The shorter durations are supported by cation diffusion estimates from other minerals in some cases, for example feldspar (Till et al., 2015) and pyroxene Chamberlain et al., 2014a). However, U-Th-Pb geochronology of zircon grains from silicic systems typically yields times of $10^4 – 10^5$ years, thought to record a long history of magma body growth and evolution prior to destabilizing events leading to eruption (e.g. Reid and Vasquez, 2017). Now, recent experiments on Ti-in-quartz diffusivity by Jollands et al. (2020) yield much slower diffusion rates than proposed by Cherniak et al. (2007), and lead to

Always consult and cite the final, published document. See http:/www.minsocam.org or GeoscienceWorld

This is the peer-reviewed, final accepted version for American Mineralogist, published by the Mineralogical Society of America.
The published version is subject to change. Cite as Authors (Year) Title. American Mineralogist, in press.
DOI: https://doi.org/10.2138/am-2020-7395. http://www.minsocam.org/

timescales for the preservation of Ti zoning profiles in quartz that are more consistent with those derived from geochronology. Thus, the status of Ti zoning in quartz as a recorder of events immediately preceding eruption is thrown into question.

In addition to zoning recorded in quartz during crystal growth, melt may become trapped as melt inclusions (MI; Fig. 1); MI are generally thought to record the liquid composition at the time of crystal growth (Lowenstern and Mahood 1991; Dunbar and Hervig 1992; Bacon et al. 1992) and are often abundant in quartz phenocrysts from rhyolites. These can then be used to make interpretations about the growth history of the quartz, and petrogenetic relations within the magma body.

This study examines measured Ti profiles in quartz phenocrysts from the Bandelier Tuff, Valles caldera, NM, USA, and compares Ti zoning with MI chemistry. Using finite-difference diffusion modeling procedures (Costa et al., 2008), the results are applied to estimating crystal residence times between initiation of overgrowth following a crystal resorption event and eruptive quenching, assuming diffusional relaxation of Ti in quartz crystals from an initial step function distribution. Melt inclusions hosted within those crystals are used to determine the petrogenetic history of the quartz. Wilcock et al. (2013) provide a detailed dataset on the CL and Ti zoning in quartz from the Tshirege Member. This study expands on those data with higher spatial resolution and MI chemistry.

GEOLOGICAL AND PETROLOGICAL BACKGROUND

The ~400 km^3 Tshirege (upper) Member of the Bandelier Tuff erupted to form the Valles caldera, Jemez Mountains, NM, USA at 1.26 Ma (Bailey et al., 1969; Phillips et al., 2007; Gardner et al., 2010; Goff et al., 2014) and has been the subject of several petrological and

Always consult and cite the final, published document. See http:/www.minsocam.org or GeoscienceWorld

This is the peer-reviewed, final accepted version for American Mineralogist, published by the Mineralogical Society of America.
The published version is subject to change. Cite as Authors (Year) Title. American Mineralogist, in press.
DOI: https://doi.org/10.2138/am-2020-7395. http://www.minsocam.org/

volcanological studies (Smith and Bailey, 1966; Self et al., 1986, 1996; Balsley, 1988; Warshaw and Smith, 1988; Caress, 1996; Stimac, 1996; Warren et al., 2007; Wilcock et al., 2013; Goff et al., 2014; Wolff et al., 2015). It is strongly compositionally zoned from early-erupted high-silica rhyolite to late-erupted low-silica rhyolite, with complex compositional variations in the last-erupted tuff (Smith and Bailey, 1966; Balsley, 1988; Goff et al., 2014; Boro, 2019). The Tshirege Member event was preceded by eruption of the similarly-sized, chemically-zoned high-silica rhyolite Otowi (lower) Member of the Bandelier Tuff at ~1.60 Ma, which formed a caldera now largely overprinted by the later eruption (Goff et al., 2011, 2014; Wolff and Ramos, 2014). During the ~340,000 y interval between the two caldera-forming events, several minor eruptions produced the Valle Toledo Member rhyolite domes and pyroclastic flow and fallout deposits of the Cerro Toledo Formation (Gardner et al., 2010).

The Tshirege Member consists of a widespread plinian fallout unit, the Tsankawi Pumice Bed, overlain by non- to densely welded ignimbrite, emplaced by numerous pyroclastic density currents (Bailey et al., 1969; Self et al., 1986, 1996). The ignimbrites are divided into mappable units, recognized over a wide area and designated Qbt1 through Qbt5 in ascending order; some numbered units are additionally subdivided (Warren et al., 2007; Goff et al., 2014). All units contain a range of compositions shown by bulk chemical analysis of single pumices and bulk tuff, representing magmas at different degrees of evolution (Balsley, 1988; Self et al., 1996; Warren et al., 2007; Goff et al., 2014). The Tshirege Member consists of volumetrically dominant high-silica rhyolite (75–79% SiO_2), low-silica rhyolite (73–75% SiO_2), and hornblende dacite with 67–71% SiO_2 (Bailey et al., 1969; Self et al., 1996; Stimac, 1996; Boro, 2019). The dacite occurs as pumice clasts scattered through most of the Tshirege Member, and may represent the recharge event that triggered the Tshirege eruption (Stimac, 1996; Goff et al., 2014;

Always consult and cite the final, published document. See http:/www.minsocam.org or GeoscienceWorld

This is the peer-reviewed, final accepted version for American Mineralogist, published by the Mineralogical Society of America.
The published version is subject to change. Cite as Authors (Year) Title. American Mineralogist, in press.
DOI: https://doi.org/10.2138/am-2020-7395. http://www.minsocam.org/

Boro et al., 2020). Goff et al. (2014) also identify an additional component of andesite in late-erupted units. Despite the overall zoned character of the Tshirege Member, there is wide variation in pumice composition at any one stratigraphic level (Self et al., 1996). Several processes, such as overturn driven by gas exsolution or thermal disturbance before eruption (Bachmann and Bergantz, 2006; Burgisser and Bergantz, 2011), extraction effects during eruption (Blake and Ivey, 1986a,b; Trial et al., 1992), or non-sequential deposition of the different magmatic components (Torres et al., 1996; Branney and Kokelaar, 2002) may limit, scramble or obscure the record of zoning in the final deposits. Hence, we find the abundances of incompatible elements in single pumice clasts to be the most useful indicators of degree of magmatic evolution and hence likely vertical position in the pre-eruptive magma body, assuming them as proxies for melt H_2O contents and hence densities. This assumption is supported by H_2O contents of melt inclusions in quartz and feldspar (Dunbar and Hervig, 1992).

Tshirege Pumice

Whole-pumice chemistry (Fig. 2) shows three distinct rhyolites were present in the Tshirege magma body at the time of eruption (Boro, 2019): two high-silica rhyolites, one enriched in incompatible trace elements (99–173 ppm Nb, 25–41ppm Th: HSR-e) and one relatively depleted in those elements (44–74 ppm Nb, 14–21 ppm Th: HSR-d), and a low-silica rhyolite (26–42 ppm Nb, 10–14 ppm Th: LSR). Quartz grains analyzed in this study were extracted from these three compositional groups of rhyolite pumice. The HSR-e is representative of the Tsankawi Pumice Bed and the lowermost part of Qbt1, and the HSR-d corresponds to the later-erupted Units Qbt2 and Qbt3 of Warren et al (2007). One additional sample, 88-1, is a

Always consult and cite the final, published document. See http:/www.minsocam.org or GeoscienceWorld

This is the peer-reviewed, final accepted version for American Mineralogist, published by the Mineralogical Society of America.
The published version is subject to change. Cite as Authors (Year) Title. American Mineralogist, in press.
DOI: https://doi.org/10.2138/am-2020-7395. http://www.minsocam.org/

hornblende dacite pumice containing quartz scavenged from rhyolite, which is texturally identical to the quartz in the rest of the rhyolite and so has been included in this study.

Quartz crystals in the Tshirege Member are frequently zoned when viewed in CL (Fig. 1). The style of zoning varies, but is dominantly 'reverse' in character, where crystal cores appear dark (lower Ti, consistent with more evolved melt or lower temperature) and rims appear bright in CL (higher Ti). Wilcock et al. (2013) describe three different CL zoning types in the Tshirege quartz: (1) reverse zoning, with varying sharpness of the boundary between CL-dark core and CL-bright rim; (2) normal zoning with a bright core and dark rim; and (3) crystals that are completely non-zoned. The full range of zoning styles and statistical analyses of their distribution in the Tshirege Member is described by Wilcock et al. (2013) and our study finds a similar distribution (Fig. 1). For the diffusion modeling portion of this study, we focus on crystals with sharp reverse zoning boundaries, which were extracted from whole pumices collected from the sub-unit Qbt3.

DATA ACQUISITION

We analyzed oriented quartz grain separates, cut normal to the *c* axis, from the Tshirege Member. Grain mounts were made using >500 μm size-fraction crystal separates. Titanium concentrations in quartz were measured by wavelength-dispersive electron probe microanalysis. Measurements were made on a JEOL JXA-8500F field emission electron microprobe located in the Peter Hooper GeoAnalytical Lab at Washington State University, using an accelerating potential of 20kV, a beam current of 400nA, and a spot size of 2-10 μm, following the procedures described by Donovan et al. (2016) for analysis of trace elements in simple matrices such as SiO_2. To summarize, measured peak X-ray intensities were corrected for continuum intensity using the mean atomic number (MAN) method of Donovan and Tingle (1996), and then

Always consult and cite the final, published document. See http:/www.minsocam.org or GeoscienceWorld

This is the peer-reviewed, final accepted version for American Mineralogist, published by the Mineralogical Society of America.
The published version is subject to change. Cite as Authors (Year) Title. American Mineralogist, in press.
DOI: https://doi.org/10.2138/am-2020-7395. http://www.minsocam.org/

184 blank corrected using the procedure of Donovan et al. (2011) to eliminate systematic errors in
185 accuracy resulting from background artifacts. Quartz crystals from Herkimer, NY, with Ti
186 concentrations of <30 ppb (Kohn and Northrup, 2009; Kidder et al., 2013) were used as a blank
187 standard. Several mounts of Herkimer quartz were prepared, so that blank standards and
188 unknowns could be carbon coated together prior to analysis to minimize differences in coating
189 thickness between blank standards and unknowns.

190 We acquired data for a cumulative time of 18 minutes using three spectrometers.
191 Titanium concentration profiles were measured with 4 or 8 μm spacing between analysis spots.
192 Measurement of [Ti] in this manner allows for detection limits of <2 ppm and analytical
193 precision (based on counting statistics) of <5% (2-sigma) for each individual measurement. This
194 combination of spot size and uncertainty is comparable to those obtained using synchotron XRF
195 on similar samples (Matthews et al., 2012; Gualda and Sutton, 2016), but with improved (i.e.,
196 shallower) depth averaging.

197 Measurements were made either on grain mounts, using quartz crystals separated from
198 the rock matrix, or in thin sections on areas far enough from adhering Ti-bearing glass or Ti-rich
199 phases, to avoid artifacts from continuum fluorescence (cf. Fournelle 2007). To minimize effects
200 arising from obliquely or randomly oriented zone boundaries and off-center sections (Shea et al.,
201 2015), crystals were mounted such that profiles were measured normal to the *c* axis across the
202 broadest part of quartz bipyramids (Fig. 1). Titanium concentration profiles ranged in length
203 from 200-400 μm and multiple profiles were acquired on some grains to test for heterogeneity
204 along CL brightness boundaries. Additionally, some profiles oblique to zone boundaries were
205 acquired and then trigonometrically corrected to obtain higher resolution across boundaries with
206 small diffusional relaxation widths. Modeling of the effects of continuum fluorescence across the

Always consult and cite the final, published document. See http:/www.minsocam.org or GeoscienceWorld

This is the peer-reviewed, final accepted version for American Mineralogist, published by the Mineralogical Society of America.
The published version is subject to change. Cite as Authors (Year) Title. American Mineralogist, in press.
DOI: https://doi.org/10.2138/am-2020-7395. http://www.minsocam.org/

boundaries between low- and high-Ti zones within the quartz crystal using PENEPMA (Llovet and Salvat, 2016) suggests that any effects of secondary fluorescence of the higher-Ti zone across the boundary are negligible (~1 ppm or less). All profiles, their model times, explanation of oblique profiles, and a comparison of multiple profiles on single crystals can be found in the supplementary data file.

Grayscale CL images were obtained using a Gatan MiniCL cathodoluminescence detector mounted on the WSU JEOL JXA-8500F using a 50 nA beam current, 10 kV, and 60 second capture time producing images with an effective image resolution of 1 μm, with constant contrast and brightness settings. ImageJ software was used to produce grayscale intensity graphs along EPMA transect lines. Under these conditions the grayscale intensities are considered internally consistent.

Titanium concentrations were also measured in a subset of quartz crystals by laser ablation inductively-coupled plasma mass spectrometry (LA-ICP-MS) to confirm the accuracy of EPMA measurements. The LA-ICP-MS measurements were performed on zones in quartz crystals that were uniformly CL-bright or CL-dark, where EPMA measurements yielded uniform Ti concentrations. Data were collected using a Teledyne Analyte Excite Excimer 193 nm laser ablation system attached to a Finnigan Element2 ICP-MS. A 20 μm spot size was used with 7 J/cm^2 beam energy, and counts collected for 30 seconds along transects that ran parallel to crystal faces and zone boundaries, staying within the zones defined by CL imaging. Calibration was achieved using NIST-612 and BCR-G glasses, plus a well-characterized internal standard quartz with 9 ppm Ti. Results of LA-ICP-MS and EPMA measurements of Ti are indistinguishable within analytical uncertainty (Table 1).

Always consult and cite the final, published document. See http:/www.minsocam.org or GeoscienceWorld

This is the peer-reviewed, final accepted version for American Mineralogist, published by the Mineralogical Society of America.
The published version is subject to change. Cite as Authors (Year) Title. American Mineralogist, in press.
DOI: https://doi.org/10.2138/am-2020-7395. http://www.minsocam.org/

Melt inclusions in quartz and external glasses in the HSR-e, HSR-d, and LSR samples were analyzed for Ti, Zn, Rb, Sr, Y, Zr, Nb, Cs, Ba, REEs, Hf, Ta, Pb, Th, and U using LA-ICP-MS. Some additional thin sections with exposed quartz melt inclusions were also analyzed. A New Wave UP-213 laser was used for ablation with a 20 Hz rep rate and laser power from 3-3.5 J/cm^2. Ablations were analyzed using a sampling rate of every ~0.9 sec with an Agilent 7700 Series quadrupole mass spectrometer. Laser track widths varied from 12-30 µm depending on available glass and melt inclusion sizes. Inclusions <50 µm in diameter were avoided. Data were normalized to NIST-610 using ^{28}Si or ^{29}Si as an internal reference.

Whole-pumice clasts were analyzed for major, minor and trace elements in the Peter Hooper GeoAnalytical Lab at Washington State University by X-ray fluorescence and inductively coupled plasma mass spectrometry (methods and procedures described at https://environment.wsu.edu/facilities/geoanalytical-lab/technical-notes/).

RESULTS

Cathodoluminescence

CL grayscale images were obtained for >50 quartz crystals. Titanium concentration profiles plus CL grayscale profiles were obtained for 20 quartz crystals from samples taken at several stratigraphic heights within the Tshirege Member. Generally, CL zoning can be split into three types (Fig. 1): 1. Non-zoned; 2. Reversely zoned; 3. Complex. In cases where there were multiple zones (e.g., Fig. 1, panel 1, 3, and 5), the outermost zone boundary was used for diffusion modeling.

Always consult and cite the final, published document. See http:/www.minsocam.org or GeoscienceWorld

This is the peer-reviewed, final accepted version for American Mineralogist, published by the Mineralogical Society of America.
The published version is subject to change. Cite as Authors (Year) Title. American Mineralogist, in press.
DOI: https://doi.org/10.2138/am-2020-7395. http://www.minsocam.org/

252

253 **Glass trace element chemistry and melt inclusion faceting**

254 Trace-element abundances in glasses are somewhat bimodal, similar to the distribution of
255 whole-pumice compositions, but do not always reflect the bulk chemistry of the clast from which
256 they were extracted (Fig. 3; full trace element glass data can be found in the supplementary data
257 file). Melt inclusions in quartz from HSR-e plot with glasses adhering to quartz crystals and
258 groundmass glass remote from crystals in thin section (collectively referred to as "external
259 glasses") from those samples. Melt inclusions from Ti-poor quartz cores in the HSR-d and LSR
260 plot with HSR-e glasses, whereas MIs that plot with HSR-d and LSR external glasses are found
261 in CL-bright rims of crystals or in crystals that show no zoning in the HSR-d or LSR. Some MIs
262 fill a gap between the two groups of data and may have trapped a liquid composition that is not
263 represented by whole-pumice data or groundmass glass data.

264 Melt inclusions occur as faceted and non-faceted forms. Faceting in melt inclusions
265 occurs as an initially round inclusion attempts to acquire a negative crystal form, accomplished
266 through lateral diffusion of silica along the edges of the inclusion (see Fig. 3 in Gualda et al.,
267 2012; supplementary file). The time that an inclusion takes to go from non-faceted to faceted is
268 positively correlated with the size of the inclusion and negatively correlated with temperature.

269 Melt inclusions in the Tshirege quartz vary from almost perfectly round to strongly
270 faceted (Fig. 4). Inclusions have been assigned a faceting strength (FS) value from 0 = unfaceted,
271 spherical inclusion to 2 = strongly faceted, negative bipyramidal crystal shape (Fig. 4d). Facet
272 strength is assigned by visual inspection of facets; the requirements for a melt inclusion to fit into
273 any individual category are outlined in Figure 4e. Although there is some subjectivity around
274 ~FS = 1.0, 0 and 0.5 are very different from 1.5 and 2. In crystals that contain multiple facets

Always consult and cite the final, published document. See http:/www.minsocam.org or GeoscienceWorld

This is the peer-reviewed, final accepted version for American Mineralogist, published by the Mineralogical Society of America.
The published version is subject to change. Cite as Authors (Year) Title. American Mineralogist, in press.
DOI: https://doi.org/10.2138/am-2020-7395. http://www.minsocam.org/

with different FS values, higher FS values are found towards the core of the crystal (Fig. 5). Barium and Sr, compatible elements in rhyolite, are correlated with the degree of faceting, where no melt inclusions above FS = 1 have Ba above ~15 ppm; FS = <1 have Ba of 5–66 ppm, with unfaceted HSR-e inclusions having the highest Ba and Sr (Fig. 4a).

Highly incompatible elements (e.g., Nb and Th) show positive correlations among all glasses (Fig. 3a). On most bivariate plots, external glasses and MIs from HSR-e pumices plot together while glasses and MIs from the HSR-d and LSR pumices plot together (Fig. 3b, c); some HSR-d and LSR MIs plot with HSR-e external glasses and MIs. Figure 3-d shows Rb/Sr vs Ba/Nb and a field of strongly faceted melt inclusions. This field contains all melt inclusions with a FS $\geq$ 1 and none with FS < 1. Generally, when faceted and unfaceted inclusions occur together in the same crystal, strongly faceted inclusions occur in the cores of crystals, where weakly or unfaceted inclusions occur in the rims. MIs plotting with external glasses from LSR and HSR-d pumices are only found in CL-bright rims and are unfaceted. The strongly faceted MIs have clearly formed from a move evolved liquid.

Faceted inclusions with a FS = 2 are 50-125 μm in radius, suggesting FS = 2 inclusions were trapped and stored in quartz for a time on the order of at least >1,000-10,000 years (Gualda et al., 2012) assuming an average storage temperature of 750 °C. Once an inclusion is strongly faceted, no further changes occur, so these are minimum times. Some of the largest (r = 150 μm) faceted melt inclusions in the Tsankawi pumice (700 °C) may have taken on the order of 10^4 years to develop (see supplementary data file for faceting times vs MI radius at different temperatures, Fig. A2).

[Ti] vs. CL grayscale intensity

Always consult and cite the final, published document. See http:/www.minsocam.org or GeoscienceWorld

This is the peer-reviewed, final accepted version for American Mineralogist, published by the Mineralogical Society of America.
The published version is subject to change. Cite as Authors (Year) Title. American Mineralogist, in press.
DOI: https://doi.org/10.2138/am-2020-7395. http://www.minsocam.org/

In Figure 6, four representative Ti concentration profiles measured across CL brightness boundaries are plotted with CL grayscale intensity, shown as 3 μm pixel averages, together with estimated times for development of each type of profile assuming an initial step function (next section). The complete set of profiles are given in the supplementary file. Resolution of Ti data at the effective spot size of 2 μm does not allow for accurate modeling of diffusional boundaries thinner than ~ 16 μm (corresponding to ~200 years diffusive relaxation at 750 °C using diffusivity coefficients from Cherniak et al., 2007) because 4-5 points are needed to define a diffusion sigmoid; however in each case the Ti slope is less steep than this limit (Fig. 6). In some cases, oblique corrected profiles allow for resolution of diffusional boundaries <16 μm (see supplementary file, sample 119-4). Usually (Fig. 6, Table 2) the CL grayscale profile is 'sharper', i.e. closer to a step function, than the Ti profile; in a few cases they are indistinguishable within uncertainty, and in two cases the Ti profile is steeper than CL grayscale, albeit still overlapping within uncertainty. To illustrate the effects of the different profiles on calculated timescale estimates (see **Modeled diffusion relaxation times** below), in Fig. 6 we compare results from CL grayscale and Ti profiles at a fixed T = 750 °C; estimates may differ by more than an order of magnitude. We now attempt to additionally estimate diffusion times from Ti profiles using temperatures derived from thermometry.

Estimation of temperature

Due to the generally high activation energies associated with cation diffusion in silicate minerals, timescales calculated from diffusion profiles are very sensitive to temperature (e.g., Cherniak et al., 2007). For example, a ΔT of ~50 °C, which is similar to the error range (i.e. ±25 °C) arising from calibration and microprobe data uncertainty for many mineral geothermometers, may result in an order of magnitude change in calculated relaxation time. It is therefore

Always consult and cite the final, published document. See http:/www.minsocam.org or GeoscienceWorld

This is the peer-reviewed, final accepted version for American Mineralogist, published by the Mineralogical Society of America.
The published version is subject to change. Cite as Authors (Year) Title. American Mineralogist, in press.
DOI: https://doi.org/10.2138/am-2020-7395. http://www.minsocam.org/

necessary to constrain temperature during diffusive relaxation as closely as possible. The Tshirege Member contains magnetite and sporadic ilmenite, but we did not find any pairs that pass the equilibrium test of Bacon and Hirschmann (1988). The first-erupted parts of both the Otowi and Tshirege Members of the Bandelier Tuff (respectively, the Guaje and Tsankawi Pumice Beds) have compositions that are close to haplogranite, are homogeneous, exhibit the least textural evidence for internal disequilibrium within their respective members, and plot very near the minimum in *Q–Ab–Or* at 2 kb H_2O saturation pressure (Wilcock et al., 2013; Wolff and Ramos, 2014), consistent with a magma temperature close to 700 °C (Tuttle and Bowen, 1958) and the measured H_2O contents of melt inclusions (Dunbar and Hervig, 1992). Warshaw and Smith (1988) give a temperature of 697 °C for the Tsankawi magma, based on an early version of the QUILF thermometer (Andersen and Lindsley, 1988), but do not report uncertainties. Wilcock et al. (2013) review several lines of evidence for storage depth of the Tshirege magma and conclude that a pressure of 200 ± 50 MPa is most appropriate. We concur and assume this pressure and a temperature of 700 °C for the Tsankawi Pumice magma.

The TitaniQ thermometer (Wark and Watson, 2006, equation 1 below; Thomas et al., 2010, equation 2 below; Huang and Audétat, 2012, equation 3 below), which relies on the temperature dependence of [Ti] in quartz, can be applied to quartz grains chosen for diffusion modeling, thus avoiding the potential problem in applying temperatures estimated from other mineral phases in high-silica rhyolites that may not be in equilibrium with quartz (Evans and Bachmann, 2013; Evans et al., 2016):

$$T(°C) = \frac{-3765 \pm 24}{\log\left(\frac{X_{Ti}^{qtz}}{a_{TiO_2}}\right) - 5.69 \pm 0.02} - 273 \quad (1)$$

$$RT\ln X_{\mathrm{TiO_2}}^{\mathrm{quartz}} = -(60952 \pm 3177) + (1.520 \pm 0.39) * T(K) - (1741 \pm 63) * P(kbar) + RT\ln a_{TiO_2}$$

Always consult and cite the final, published document. See http:/www.minsocam.org or GeoscienceWorld

This is the peer-reviewed, final accepted version for American Mineralogist, published by the Mineralogical Society of America.
The published version is subject to change. Cite as Authors (Year) Title. American Mineralogist, in press.
DOI: https://doi.org/10.2138/am-2020-7395. http://www.minsocam.org/

343 (2)

344 $$\log \mathrm{Ti(ppm)} = -0.27943 * \frac{10^4}{T} - 660.53 * \frac{P^{0.35}}{T} + 5.6459 \quad (3)$$

345 In each case, the thermometer is experimentally calibrated for melts saturated with rutile,
346 hence $a(TiO_2)_{melt} = 1$; the chief difficulty in its application therefore lies in the estimation of
347 $a(TiO_2)_{melt}$ because the vast majority of volcanic silicate liquids are not rutile-saturated. Hayden
348 and Watson (2007) provide a method for estimating $a(TiO_2)_{melt}$ based on rutile saturation as a
349 function of melt composition and temperature; however this is only calibrated at 1 GPa, at which
350 pressure rutile solubility is likely less than at the mid- to upper-crustal storage depths of most
351 rhyolites (Thomas and Watson, 2012). Rhyolite-MELTS (Gualda et al., 2012) calculates
352 $a(TiO_2)_{melt}$ but the values for the exceptionally Ti-poor glasses of the Tshirege Member are
353 extremely low (~10^{-5}), yielding unreasonably high temperatures.

354 Instead, we have calculated $a(TiO_2)_{melt}$ for the Tshirege Member by 'internally
355 calibrating' to an assumed temperature of 700 °C for the first-erupted Tsankawi pumice, and
356 setting $a(TiO_2)_{melt}$ to a value of 0.34, which yields 700 °C for the average compositions of
357 Tsankawi quartz (~22.5 ppm Ti) using Eqn. (1). The same result is obtained from the Huang and
358 Audétat (2012) calibration (Eqn. 3) using this $a(TiO_2)_{melt}$ if P is set to 263 MPa. The high-
359 pressure Thomas et al. (2010) calibration (Eqn. 2) requires a different $a(TiO_2)_{melt}$ of 0.0775, and
360 was not used here. The Tsankawi-derived $a(TiO_2)_{melt}$ value is then treated in two ways. In the
361 first approach, $a(TiO_2)$ is assumed constant throughout the Tshirege Member high-silica rhyolite
362 magma. This assumption can be justified on the basis that titanomagnetite is a ubiquitous, if
363 trace, phenocryst phase (Warren et al., 2007) and hence may buffer $a(TiO_2)_{melt}$. However, it is
364 unclear whether or not quartz and titanomagnetite were co-precipitating phases, or whether
365 titanomagnetite compositions or abundances may have changed during quartz growth, an issue

Always consult and cite the final, published document. See http:/www.minsocam.org or GeoscienceWorld

This is the peer-reviewed, final accepted version for American Mineralogist, published by the Mineralogical Society of America.
The published version is subject to change. Cite as Authors (Year) Title. American Mineralogist, in press.
DOI: https://doi.org/10.2138/am-2020-7395. http://www.minsocam.org/

366 that has led to conflicting interpretations of temperature estimates for the Bishop Tuff, a similar
367 voluminous high-silica rhyolite eruption (Evans and Bachmann, 2013; Gualda and Ghiorso,
368 2013; Evans et al., 2016; Jolles and Lange, 2019). Therefore, when estimating $a(TiO_2)_{melt}$ for the
369 Tshirege Member magmas, buffering cannot be assumed. Instead, the $a(TiO_2)_{melt}$ value of 0.34 is
370 used to calculate an effective TiO_2 activity coefficient for measured TiO_2 in Tsankawi glasses,
371 which is then applied to compositions of glasses in contact with quartz rims throughout the
372 Tshirege Member. The assumption of constant $\gamma(TiO_2)_{melt}$, where γ denotes the activity
373 coefficient, is justified by the essentially constant major-element composition of Tshirege high-
374 silica rhyolite.

375 Modeled diffusion relaxation times (next section) are calculated using three different
376 temperature assumptions: (i) constant temperature of 750 °C (Fig. 6); (ii) temperature estimated
377 using the Wark and Watson (2006) and Huang and Audétat (2012) calibrations at 263 MPa,
378 assuming constant $a(TiO_2)_{melt}$; (iii) temperature estimated using the Wark and Watson (2006)
379 and Huang and Audétat (2012) calibrations at 263 MPa, and applying calculated $\gamma(TiO_2)_{melt}$ to Ti
380 contents of glasses adhering to quartz crystals to estimate $a(TiO_2)_{melt}$. In cases (ii) and (iii), the
381 temperature calculated from the rim composition of the quartz is assumed to apply to diffusion at
382 the inner boundary of the rim.

383

384 **Modeled diffusion relaxation times**

385 We use the 1-D finite difference diffusion method (Costa et al., 2008, equation 4 below),
386 to model Ti diffusion in quartz as a function of time and distance of travel in the lattice:

387 $$C_{i,j+1} = C_{i,j} + \left(\frac{D\Delta t\left(C_{i+1,j} - 2C_{i,j} + C_{i-1,j}\right)}{\Delta x^2}\right) \qquad (4)$$

Always consult and cite the final, published document. See http:/www.minsocam.org or GeoscienceWorld

This is the peer-reviewed, final accepted version for American Mineralogist, published by the Mineralogical Society of America.
The published version is subject to change. Cite as Authors (Year) Title. American Mineralogist, in press.
DOI: https://doi.org/10.2138/am-2020-7395. http://www.minsocam.org/

Where: $C_{i,j}$ = the concentration at the current lattice location; $C_{i,j+1}$ = the concentration at the current lattice location one time step forward; $C_{i+1,j}$ = the concentration one lattice step towards the diffusion zone; $C_{i-1,j}$ = the concentration one lattice step away from the diffusion zone; D = diffusion coefficient for the diffusing species in lattice of interest; Δt = change in time for one step in the model; Δx = step size. Boundary conditions for the high and low steps at time = 0 were set as the average [Ti] outside of the diffusive relaxation zone, where data formed a plateau, or in cases where data did not form a good plateau, the boundary condition was set to a best fit line through boundary data.

The diffusion coefficient of Ti in quartz parallel to the *c* axis is not well established and we use the two current published values given by (Cherniak et al., 2007, equation 5; Jollands et al., 2020, equation 6):

$$D_{\mathrm{Ti}} = 7 \times 10^{-8} \exp(-273 \pm 12 \text{ kJ mol}^{-1} / RT) \text{ m}^2 \text{ sec}^{-1} \quad (5)$$

$$log_{10} D_{\mathrm{Ti}} = -8.3 \pm 0.4 - [311 \pm 12 \text{ kJ mol}^{-1} / (2.303 RT)] \text{ m}^2 \text{ sec}^{-1} \quad (6)$$

Where: D_{Ti} = diffusion coefficient of Ti in quartz, R is the universal gas constant and T is absolute temperature. Cherniak et al. (2007) provide seven additional experiments measuring Ti diffusion in quartz normal to *c*, with little anisotropy apparent. Regression of those experiments over the temperature range 750 – 1101 °C gives an Arrhenius relation that yields results indistinguishable from Eqn (5), which we use here and suggests that Ti-diffusion parallel or perpendicular to *c*-axes is similar. Errors for the CL and Ti profiles at constant temperatures are calculated from the inherent error in the D_{Ti} which, when applied to these data, lead to large (40-60%) errors of modeled times. In Table 2, uncertainties of diffusion times for the Ti profiles calculated using temperatures from TitaniQ that arise from fitting sigmoids to the data are

Always consult and cite the final, published document. See http:/www.minsocam.org or GeoscienceWorld

This is the peer-reviewed, final accepted version for American Mineralogist, published by the Mineralogical Society of America.
The published version is subject to change. Cite as Authors (Year) Title. American Mineralogist, in press.
DOI: https://doi.org/10.2138/am-2020-7395. http://www.minsocam.org/

411 reported separately. The very different diffusivities from Cherniak et al. (2007) and Jollands et
412 al. (2020) result in diffusion timescales that are systematically offset by an average of two orders
413 of magnitude (Figure 6; Tables 2 and 3); the implications of these results are outlined in the
414 **Discussion** section below.

415 In most cases, Ti diffusive relaxation times calculated from CL grayscale profiles are
416 shorter than those calculated from Ti data using the same D_{Ti}, by up to an order of magnitude
417 (Table 2, Fig. 6). In some cases the two profiles yield identical results within error. Previous
418 authors have presented discrepant CL grayscale and Ti concentration data, consistent with our
419 findings (e.g., Fig. 9 of Matthews et al., 2012), but have discounted the significance for
420 calculated timescales. We also note that, overall, grayscale profiles are smoother than those for
421 Ti concentrations from the same crystal (Fig. 6), resulting in many cases in decreased, but
422 perhaps less realistic, calculated uncertainties associated with timescales (Table 2). Furthermore,
423 while spectroscopic measurements of quartz CL emissions at specific wavelengths, such as ~454
424 nm, are very well correlated with Ti contents (MacRae et al., 2013, 2018), greyscale CL is not a
425 reliable proxy for Ti concentration. For many panchromatic CL detectors, the collection optics
426 accept light from a wide variety of angles, and therefore light from adjacent areas, which are still
427 emitting from the initial electron bombardment, or light transmitted through the sample and
428 scattered off of microcracks in the sample, which may be included in a CL measurement that is
429 supposed to represent only the CL emitted from an individual pixel (MacRae et al., 2013). Also,
430 as described by Leeman et al. (2012) and MacRae et al. (2018), greyscale intensities include not
431 only CL from Ti dopants, but also from the intrinsic CL produced by quartz, by crystallographic
432 defects, by aluminum dopants, and by non-bridging oxygen holes in the crystal structure. In fact,
433 certain CL emissions from quartz, such as those from non-bridging oxygen holes, are actually

Always consult and cite the final, published document. See http:/www.minsocam.org or GeoscienceWorld

This is the peer-reviewed, final accepted version for American Mineralogist, published by the Mineralogical Society of America.
The published version is subject to change. Cite as Authors (Year) Title. American Mineralogist, in press.
DOI: https://doi.org/10.2138/am-2020-7395. http://www.minsocam.org/

434 *inversely* correlated with Ti contents (see Fig. 4 of Leeman et al., 2012). Therefore, the diffusion
435 profiles used for the modeling presented here are based on the Ti concentrations measured by
436 EPMA; profiles based on CL intensity are not considered.

437

438 **DISCUSSION**

439 Titanium concentrations in rims of zoned quartz are invariably higher than those in
440 Tsankawi quartz, hence estimated temperatures are always higher. Assuming 700 °C for the
441 Tsankawi, the average temperature (excluding dacite 88-1) for quartz rims in pumice clasts with
442 64 – 73 ppm Nb is 774 ± 14 °C ($a(TiO_2)$ method) or 740 ± 17 °C ($\gamma(TiO_2)$ method). This
443 reinforces the qualitative value of the TitaniQ thermometer, but the difficulties associated with
444 $a(TiO_2)$ estimation somewhat negate its quantitative value as a thermometer applicable to
445 rhyolites (see also Wilson et al., 2012). The majority of rhyolites with high magmatic H_2O
446 contents erupt at temperatures between 700 and 800 °C, so the temperature estimates in Table 2
447 are reasonable but hardly surprising.

448 Sample 88-1 is a hornblende dacite pumice containing quartz texturally indistinguishable
449 from that in the high-silica rhyolite (Fig. 1); the quartz is thought to have been incorporated as
450 dacite mixed with rhyolite immediately prior to the eruption (Stimac, 1996; Boro et al., 2020).
451 The quartz rim compositions yield temperatures of 799–825 °C, consistent with 797 ± 17 °C
452 from amphibole thermometry (Boro et al., 2020). Despite the higher temperature, this quartz
453 crystal produces one of the longest modeled Ti diffusion times (see 750 °C Ti model-time
454 column, Table 2), and hosts a FS = 2 melt inclusion in the CL-dark core, supporting a long
455 storage time for this crystal.

Always consult and cite the final, published document. See http:/www.minsocam.org or GeoscienceWorld

This is the peer-reviewed, final accepted version for American Mineralogist, published by the Mineralogical Society of America.
The published version is subject to change. Cite as Authors (Year) Title. American Mineralogist, in press.
DOI: https://doi.org/10.2138/am-2020-7395. http://www.minsocam.org/

There is a large discrepancy between the widely-used values of D_{Ti} in quartz of Cherniak et al. (2007), and the recent estimate of Jollands et al. (2020); compare eqns (5) and (6). Use of eqn. (5) has produced estimates of short timescales for quartz regrowth (Matthews et al., 2012; Till et al., 2015; Gualda and Sutton, 2016; Cooper et al., 2017), although in some cases these timescales are supported by other methods (e.g., Chamberlain et al., 2014a). In the case of the Tshirege Member, the Jollands et al. (2020) diffusivities yield modeled diffusion times of chemical relaxation across growth boundaries in quartz up to 10^7 years (Table 3), which is geologically unreasonable for this system; we take the 360 k.y. time between the Otowi and Tshirege eruptions as the maximum geologically reasonable timescale for crystal growth likely to be recorded in the Tshirege Member. Most of the estimates in Table 3 are longer.

Therefore, if the Jollands et al. (2020) diffusion coefficients (Eqn. 6) are preferred, the assumption of an initial step-function Ti concentration profile may be invalid, and the profiles in Fig. 6 are partly inherited from crystal growth. In this case the initial condition is not constrained. Although diffusion sigmoids can be fit to all cases, in detail both the CL and Ti concentration profiles show numerous minor reversals and irregularities on either side of the zone boundary. Commonly, a thin peak in Ti or Cl brightness occurs of the high-Ti side of the boundary (Fig. 6; supplemental data). These variations may be due to changes in crystal growth rate (Huang and Audétat, 2012). However, the major CL dark core – CL light rim boundary often truncates earlier zoning in the crystal core, so is not solely a result of changes in growth rate but is the product of an episode of resorption followed by regrowth. The presence of unfaceted melt inclusions in many crystals, including some of the CL-bright crystal rims, limits their residence at magmatic temperature to less than ~2 x 10^4 years (supplementary data), using the faceting time estimation of Gualda et al. (2012; their eqn. 9). In addition to the overall

Always consult and cite the final, published document. See http:/www.minsocam.org or GeoscienceWorld

This is the peer-reviewed, final accepted version for American Mineralogist, published by the Mineralogical Society of America.
The published version is subject to change. Cite as Authors (Year) Title. American Mineralogist, in press.
DOI: https://doi.org/10.2138/am-2020-7395. http://www.minsocam.org/

chronology of the Bandelier system, this also militates against the timescales estimated using Eqn. (6), and assuming an initial step function, having any geological meaning.

If the Cherniak et al. (2007) diffusion coefficients (eqn. 5) are preferred, the results suggest that an event or events involving reheating of the system occurred over a range between <100 and >1,000 years (order of magnitude) prior to eruption, generally consistent with melt inclusion faceting times. These events preceded recharge by the dacite, which may have acted as the trigger for the eruption (Stimac, 1996; Goff et al., 2014; Boro et al., 2020) on a shorter timescale. Some quartz crystals (Fig. 1) have rounded edges and appear to have gone through an additional resorption event, truncating existing zoning patterns, without subsequent growth of new quartz prior to the eruption, so the calculated times in Table 2 may reflect a sequence of events cascading towards the caldera-forming eruption.

The reasons for the large contrast between fast and slow diffusivities estimated by Cherniak et al. (2007) and Jollands et al. (2020) respectively is unclear. Each study uses a experimentally similar method of exposing quartz to a powdered source of TiO_2 followed by depth profiling, with the major differences being that Cherniak et al. (2007) used a 99.9% pure TiO_2 source for Ti and Jollands et al. (2020) used a Ti-doped SiO_2 powder with [Ti] of ~100 ppm. Jollands et al. (2020) were unable to reproduce the results of Cherniak et al. (2007) using a pure TiO_2 source due to degradation of the quartz crystal surface during a one-hour annealing with a pure rutile powder, making subsequent depth profiling using SIMS unfeasible. Jollands et al. (2020) speculate that Ti may have more than one diffusion mechanism in quartz, with the faster mechanism effectively absent at the low Ti concentrations of their experiments (see their supplemental file p. 10), and therefore, by implication, in the majority of natural cases. The

Always consult and cite the final, published document. See http:/www.minsocam.org or GeoscienceWorld

This is the peer-reviewed, final accepted version for American Mineralogist, published by the Mineralogical Society of America.
The published version is subject to change. Cite as Authors (Year) Title. American Mineralogist, in press.
DOI: https://doi.org/10.2138/am-2020-7395. http://www.minsocam.org/

question of which diffusivities are more correct has significant implications for understanding the dynamics and timescales for silicic magma systems. Our study does not resolve this question.

IMPLICATIONS

Compositional zoning of the Tshirege Member magma

Most quartz cores from HSR-d pumice have near-constant and low Ti contents, indistinguishable from non-zoned quartz in HSR-e Tsankawi pumice. The MIs hosted by these cores are typically faceted and have trace element abundances similar to HSR-e pumice, whereas the occasional MIs in the Ti-rich rims of quartz from HSR-d pumice have HSR-d chemistry and are non- or weakly faceted (Fig. 5). These observations link overall bulk zoning in the Tshirege Member to melt inclusion chemistry (Figs. 2, 3), quartz growth, and quartz residence time. The most evolved, first-erupted melt compositions (HSR-e chemistry) and low-Ti quartz existed *before* the less evolved, late-erupted melt (HSR-d and LSR chemistries) and high-Ti quartz developed in the erupted portion of the system. This is consistent with a simple model of crystallization, cumulate formation, and subsequent melting and remobilization of the cumulate to create a compositionally zoned magma body (Wolff et al., 2015, 2020). In this model, which is an extension of the 'mush model' (Bachmann and Bergantz, 2004; Hildreth, 2004), the quartz-feldspar cumulate pile beneath a cognate crystal-poor melt lens is heated and remobilized by recharge, with little mass contribution from the recharge magma (Wark et al., 2007; Wolff and Ramos, 2014). The result is a relatively water-poor rhyolite, of higher density and with lower incompatible element concentrations than the initial rhyolite melt lens. The new melt, with a cargo of crystals inherited from the cumulate pile, pools beneath the initial melt lens to form a thicker, compositionally zoned body of eruptible magma. The lack of quartz zoning in HSR-e

Always consult and cite the final, published document. See http:/www.minsocam.org or GeoscienceWorld

This is the peer-reviewed, final accepted version for American Mineralogist, published by the Mineralogical Society of America.
The published version is subject to change. Cite as Authors (Year) Title. American Mineralogist, in press.
DOI: https://doi.org/10.2138/am-2020-7395. http://www.minsocam.org/

524 samples suggests an enriched liquid lens that was shut off from the thermal and chemical effects
525 of invading recharge magmas, likely shielded by a crystal mush that was melted and mobilized to
526 form the HSR-d magma.

527 Figure 7 depicts four stages in the development of zoning in the Tshirege system:

528 a. Initial state of the system is an accumulating crystal mush overlain by a lens of
529 magma, which is highly enriched in incompatible trace elements, and depleted in
530 compatible trace elements – especially those which strongly partition into sanidine
531 (i.e., Sr and Ba). This system is producing quartz crystals that trap melt from the
532 evolved body and settle to contribute to the mush.
533 b. The mush is around 70% crystallinity with correspondingly lower bulk water content
534 then the melt and consists of crystals with melt inclusions. Storage for 1,000-10,000
535 years allows for faceting of melt inclusions.
536 c. Recharge magma, underplating and intruding the crystal mush column, acts as a
537 heating element and may also add H_2O to the system from second boiling, loosening
538 the mechanically locked mush (Boro, 2019), causing quartz crystals to partially
539 resorb. Simultaneous melting of feldspar adds Ba and Sr to the melt. Crystals resume
540 growing.
541 d. Quartz crystals regrow as they find a new equilibrium at higher temperatures forming
542 CL-bright rims with higher Ti concentrations, and capture the recharge event with
543 unfaceted melt inclusions enriched in Ba and Sr. Continued recharge of the system
544 mobilizes the mush and overpressure triggers the eruption.

545

Always consult and cite the final, published document. See http:/www.minsocam.org or GeoscienceWorld

This is the peer-reviewed, final accepted version for American Mineralogist, published by the Mineralogical Society of America.
The published version is subject to change. Cite as Authors (Year) Title. American Mineralogist, in press.
DOI: https://doi.org/10.2138/am-2020-7395. http://www.minsocam.org/

Eruption forecasting

An important application of petrologic study of past eruptions is to draw links between events recorded in crystals and melts, particularly those interpreted as destabilizing to the system, and monitoring signals that might be detected at the surface in the run-up to a future eruption (Blundy and Cashman, 2008). Studies using the Cherniak et al. (2007) Ti-in-quartz diffusion coefficients (e.g., Gualda and Sutton, 2016; Cooper et al., 2017) have emphasized short timescales of crystal regrowth and residence following recharge events prior to a supereruption. In the case of the Tshirege Member, the events recorded in quartz would imply multiple disturbances over ~10^3 years prior to eruption, culminating in the intrusion of dacite magma into the system, the probable immediate trigger for the eruption (Goff et al., 2014; Boro et al., 2020). If recharge events can be detected at the surface (e.g., inflation, seismicity, increased gas flux), it is unclear how the critical eruption trigger could be identified, but a series of events over a long term might indicate destabilization of a static magma body. The new diffusion coefficients of Jollands et al. (2020) immediately throw all the short timescale estimates derived by previous workers from Ti (or CL) profiles in quartz into question. Jollands et al. (2020) note that the longer timescales of $10^{5\pm1}$ y they calculate for quartz residence and growth in the Bishop Tuff are consistent with the durations of magma reservoir assembly derived from zircon U-Th-Pb dating and other methods. We may note that both short and long timescales for the Bishop Tuff - Long Valley system are currently supported by other methods: short times (<10^2 years, Wark et al., 2007, using the Cherniak et al., 2007 diffusivities) are supported by diffusion-based estimates from other phases (Chamberlain et al., 2014a) and long times (~10^5 years, Jollands et al., 2020, using their diffusivities) by radioisotope studies of zircon (Coath and Reid, 2000; Simon and Reid, 2005; Chamberlain et al., 2014b). Regardless of which Ti diffusivities are correct, an

Always consult and cite the final, published document. See http:/www.minsocam.org or GeoscienceWorld

This is the peer-reviewed, final accepted version for American Mineralogist, published by the Mineralogical Society of America.
The published version is subject to change. Cite as Authors (Year) Title. American Mineralogist, in press.
DOI: https://doi.org/10.2138/am-2020-7395. http://www.minsocam.org/

overall picture of silicic systems being established over ~10^5 years or longer, and subject to multiple disturbances such as recharge which ultimately lead to eruption, seems robust; the question that remains is what exactly quartz is telling us about this history.

Our results from the Tshirege Member suggest that the longer Ti-in-quartz duration estimates may be incorrect, not necessarily because the diffusivity experiments are flawed, but more probably because the assumption of an initial sharp Ti-zone boundary in quartz is invalid. The agreement of shorter times obtained using the diffusivity value published by Cherniak et al. (2007) with melt-faceting times is also notable. We conclude that, without constraints on initial conditions, Ti profiles in quartz shed no light on the timescales for destabilization and mobilization of rhyolitic magma bodies preparatory to eruption until this current discrepancy is sufficiently addressed.

ACKNOWLEDGEMENTS

This work was funded by NSF EAR-0810306 and Washington State University. We thank Tom Shea, Ren Thompson, Fraser Goff, Steve Self and the late Jamie Gardner for discussion, Will Nachlas for providing the Herkimer quartz crystals, and Scott Boroughs, Charles Knaack, Ashley Steiner, Suzy Krahn and Kamilla Fellah for assistance in field and laboratory. The paper was improved thanks to reviews by an anonymous reviewer and Fabio Arzilli.

Always consult and cite the final, published document. See http:/www.minsocam.org or GeoscienceWorld

This is the peer-reviewed, final accepted version for American Mineralogist, published by the Mineralogical Society of America.
The published version is subject to change. Cite as Authors (Year) Title. American Mineralogist, in press.
DOI: https://doi.org/10.2138/am-2020-7395. http://www.minsocam.org/

588 **REFERENCES CITED**

589 Anderson, D.J., Lindsley, D.H. (1988) Internally consistent solution models for Fe-Mg-Mn-Ti
590 oxides; Fe-Ti oxides. American Mineralogist 73, 714-726.
591 Arzilli et al. 2019. The unexpected explosive sub-Plinian eruption of Calbuco volcano
592 (22–23 April 2015; southern Chile): Triggering mechanism implications. Journal of
593 Volcanology and Geothermal Research 378 (2019): 35-50.
594 Bachmann, O., Bergantz, G.W. (2004) On the Origin of Crystal-poor Rhyolites: Extracted from
595 Batholithic Crystal Mushes. Journal of Petrology 45-8, 1565-1582.
596 Bachmann, O., Bergantz, G.W. (2006) Gas percolation in upper-crustal silicic crystal mushes as
597 a mechanism for upward heat advection and rejuvenation of near-solidus magma bodies.
598 Journal of Volcanology and Geothermal Research, 149, 85-102.
599 Bacon, C.R. and Hirschmann, M.M. (1988) Mg/Mn partitioning as a test for equilibrium between
600 coexisting Fe-Ti oxides. American Mineralogist, 73, 57–61.
601 Bacon, C.R., Newman, S., Stopler, E.M. (1992) Water, CO2, Cl, and F in melt inclusions in
602 phenocrysts from three Holocene explosive eruptions, Crater Lake, Oregon. American
603 Mineralogist, 77(9-10), 1021-1030.
604 Bailey, R.A., Smith, R.L. and Ross, C.S. (1969) Stratigraphic nomenclature of volcanic rocks in
605 the Jemez Mountains, New Mexico. U.S. Geological Survey Bulletin, 1274-P, 1–19.
606 Balsley, S.D. (1988) The petrology and geochemistry of the Tshirege Member of the Bandelier
607 Tuff, Jemez Mountains volcanic field, New Mexico, U.S.A. M.S. thesis, University of Texas
608 at Arlington, 188 p.
609 Blake, S., Ivey, G.N. (1986a) Magma-mixing and the dynamics of withdrawal from stratified
610 reservoirs. Journal of Volcanology and Geothermal Research, 27, 153-178.
611 Blake, S., Ivey, G.N. (1986b) Density and viscosity gradients in zoned magma chambers, and
612 their influence withdrawal dynamics. Journal of Volcanology and Geothermal Research, 30,
613 201-230.
614 Blundy, J., Cashman, K. (2008) Petrologic Reconstruction of Magmatic System Variables and
615 Processes. Reviews in Mineralogy and Geochemistry 69, 179-239.

Always consult and cite the final, published document. See http:/www.minsocam.org or GeoscienceWorld

This is the peer-reviewed, final accepted version for American Mineralogist, published by the Mineralogical Society of America.
The published version is subject to change. Cite as Authors (Year) Title. American Mineralogist, in press.
DOI: https://doi.org/10.2138/am-2020-7395. http://www.minsocam.org/

Boro, J.R. (2019) Recharge and mobilization of crystal mush to produce and erupt a zoned magma chamber – the Tshirege Member of the Bandelier Tuff, Valles caldera, New Mexico, USA: Ph.D. dissertation, Washington State University.

Boro, J.R., Wolff, J.A. and Neill, O.K. (2020) Anatomy of a recharge magma: Hornblende dacite pumice from the rhyolitic Tshirege Member of the Bandelier Tuff, Valles caldera, New Mexico, USA. Submitted to Contributions to Mineralogy and Petrology.

Branney, M.J. and Kokelaar, P. (2002) Pyroclastic Density Currents and the Sedimentation of Ignimbrites. Geological Society. Geological Society Memoir, 27, 143 pp.

Burgisser, A., Bergantz, G.W. (2011). A rapid mechanism to remobilize and homogenize highly crystalline magma bodies. Nature, 471, 212-215.

Campbell, M.E., Hanson, J.B., Minarik, W.G., and Stix, J. (2009) Thermal history of the Bandelier magmatic system: evidence for magmatic injection and recharge at 1.61 Ma as revealed by cathodoluminescence and titanium geothermometry. Journal of Geology, 117, 469–485.

Caress, M.E. (1996) Zonation of alkali feldspar compositions in the Tshirege Member of the Bandelier Tuff in Pueblo Canyon, near Los Alamos, New Mexico. New Mexico Geological Society, 47th Field Conference Guidebook, 275–283.

Chamberlain, K.J., Morgan, D.J., and Wilson, C.J.N. (2014a) Timescales of mixing and mobilisation in the Bishop Tuff magma body: perspectives from diffusion chronometry. Contributions to Mineralogy and Petrology, 168:1034, 24 pp.

Chamberlain, K.J., Wilson, C.J.N., Wooden, J.L., Charlier, B.L.A., and Ireland, T.R. (2014b) New perspectives on the Bishop Tuff from zircon textures, ages and trace elements. Journal of Petrology, 55, 395–426.

Cherniak, D.J., Watson, E.B, and Wark., D.A. (2007) Ti diffusion in quartz. Chemical Geology, 236, 65–74.

Cooper, G.F., Morgan, D.J., and Wilson, C.J.N. (2017) Rapid assembly and rejuvenation of a large silicic magmatic system: insights from mineral diffusive profiles in the Kidnappers and Rocky Hill deposits, New Zealand. Earth and Planetary Science Letters, 473, 1–13.

Costa, F. and Dungan M.A. (2005) Short timescales of magmatic assimilation from diffusion modelling of multiple elements in olivine. Geology, 33, 837–840.

Always consult and cite the final, published document. See http:/www.minsocam.org or GeoscienceWorld

Costa, F., Dohmen, R., and Chakraborty, S. (2008) Time scales of magmatic processes from modeling the zoning patterns of crystals. Reviews in Mineralogy and Geochemistry, 69, 545–594.

Donovan, J.J., Lowers, H.A., and Rusk, B.G. (2011) Improved electron probe microanalysis of trace elements in quartz. American Mineralogist, 96, 274–282.

Donovan, J.J., Singer, J.W. and Armstrong, J.T. (2016). A new EPMA method for fast trace element analysis in simple matrices. American Mineralogist, 101, 1839–1853.

Donovan, J.J., Tingle, T.N., 1996. An improved mean atomic number background correction for quantitative microanalysis. J. Microsc. Soc. Am. 2, 1-7.

Dunbar, N.W and Hervig, R.L. (1992) Volatile and trace element composition of melt inclusions from the lower Bandelier Tuff; implications for magma chamber processes and eruptive style. Journal of Geophysical Research, 97, 15,151-15,170.

Evans, B.W. and Bachmann, O. (2013) Implications of equilibrium and disequilibrium among crystal phases in the Bishop Tuff. American Mineralogist, 98, 271–274.

Evans, B.W., Hildreth, W., Bachmann, O., and Scaillet, B. (2016) In defense of magnetite-ilmenite thermometry in the Bishop Tuff and its implication for gradients in silicic magma reservoirs. American Mineralogist, 101, 469–482.

Fournelle, J.F. (2007) The Problem of Secondary Fluorescence in EPMA in the Application of the Ti-in-Zircon Geothermometer and the Utility of PENEPMA Monte Carlo Program. Microscopy and Microanalysis, 13(S02), 1390-1391. doi: 10.1017/S1431927607079354

Gardner, J.N., Goff, F., Kelley, S.A. and Jacobs, E. (2010) Rhyolites and associated deposits of the Valles-Toledo caldera complex. New Mexico Geology, 32, 3–18.

Goff, F., Gardner, J.N., Reneau, S.L., Kelley, S.A., Kempter, K.A., and Lawrence, J.R. (2011) Geologic map of the Valles caldera, Jemez Mountains, New Mexico. New Mexico Bureau of Geology and Mineral Resources Geologic Map, 79, scale 1:50,000.

Goff, F., Warren, R.G., Goff, C.J., and Dunbar, N. (2014) Eruption of reverse-zoned upper Tshirege member, Bandelier Tuff from centralized vents within Valles caldera, New Mexico. Journal of Volcanology and Geothermal Research, 276, 82–104.

Götze, J. (2012) Application of cathodoluminescence microscopy and spectroscopy in geosciences. Microscopy and Microanalysis, 18, 1270–1284.

Gualda, A.R.G, Sutton, S.R. (2016) The Year Leading to a Supereruption. PLoS ONE 11, 18pp.

This is the peer-reviewed, final accepted version for American Mineralogist, published by the Mineralogical Society of America.
The published version is subject to change. Cite as Authors (Year) Title. American Mineralogist, in press.
DOI: https://doi.org/10.2138/am-2020-7395. http://www.minsocam.org/

677 Gualda, G.A.R, Pamukcu, A.S., Ghiorso, M.S., Anderson, A.T Jr., Sutton, S.R., Rivers, M.L.
678 (2012) Timescales of Quartz Crystallization and the Longevity of the Bishop Giant Magma
679 Body. PLoS ONE 7(5).
680 Gualda, G.A.R. and Ghiorso, M.S. (2013) The Bishop Tuff giant magma body: an alternative to
681 the standard model. Contributions to Mineralogy and Petrology, 166, 755–775.
682 Hayden, L.A. and Watson, E.B. (2007) Rutile saturation in hydrous siliceous melts and its
683 bearing on Ti-thermometry of quartz and zircon. Earth and Planetary Science Letters, 258,
684 561–568.
685 Hildreth, W. (2004) Volcanological perspectives on Long Valley, Mammoth Mountain, and
686 Mono Craters: several contiguous but discrete systems. Journal of Volcanology and
687 Geothermal Research 136, 169-198.
688 Huang, R. and Audétat, A. (2012) The titanium-in-quartz (TitaniQ) thermombarometer: a critical
689 examination and re-calibration. Geochimica et Cosmochimica Acta, 84, 75–89.
690 Jollands, M.C., Bloch, E., and Müntener, O. (2020) New Ti-in-quartz diffusivities reconcile
691 natural Ti zoning with time scales and temperatures of upper crustal magma reservoirs.
692 Geology 48, doi:10.1130/G47238.1
693 Jolles, J.S.R. and Lange, R.A. (2019) High-resolution Fe-Ti oxide thermometry applied to
694 single-clast pumices from the Bishop Tuff: a re-examination of compositional variations in
695 phenocryst phases with temperature. Contributions to Mineralogy and Petrology 174:70, 43
696 pp.
697 Kidder, S., J.-P. Avouac and Y.-C. Chan (2013), Application of titanium-in-quartz
698 thermobarometry to greenschist facies veins and recrystal-lized quartzites in the Hsuehshan
699 range, Taiwan, Solid Earth, 4(1), 1–21, doi:10.5194/se-4-1-2013
700 Kohn MJ, Northrup CJ. 2009. Taking mylonites' temperature. Geology 37(1), 47–50
701 Leeman, W.P., MacRae, C.M., Wilson, N.C., Torpy, A., Lee, C.-T.A., Student, J.J., Thomas,
702 J.B., and Vicenzi, E/P. (2012) A study of cathodoluminescence and trace element
703 compositional zoning in natural quartz from volcanic rocks: mapping titanium content in
704 quartz. Microscopy and Microanalysis, 18, 1322–1341.
705 Llovet, X., and Salvat, F. (2016) PENEPMA: a Monte Carlo programme for the simulation of X-
706 ray emission in EPMA. IOP Conf. Ser.: Mater. Sci. Eng.109012009

Always consult and cite the final, published document. See http:/www.minsocam.org or GeoscienceWorld

This is the peer-reviewed, final accepted version for American Mineralogist, published by the Mineralogical Society of America.
The published version is subject to change. Cite as Authors (Year) Title. American Mineralogist, in press.
DOI: https://doi.org/10.2138/am-2020-7395. http://www.minsocam.org/

Lowenstern, J.B., Mahood, G.A. (1991) New data on magmatic H2O contents of pantellerites, with implications for petrogenesis and eruptive dynamics at Pantelleria. Bulletin of Volc. 57-1, 78-83.

MacRae, C.M., Wilson, N.C., Torpy, A. (2013) Hyperspectral cathodoluminescence. Mineralogy & Petrology 107, 429-440. Doi: 10.1007/s00710-013-0272-8

MacRae, C.M., Wilson, N.C., Torpy, A., and Delle Piane, C. (2018) Soft X-ray and cathodoluminescence measurement, optimization and analysis at liquid nitrogen temperatures. IOP Conference Series: Materials Science and Engineering, Volume 304, Issue 1, pp. 012010 (2018).

Matthews, N.E., Huber, C., Pyle, D.M., and Smith, V.V. (2012) Timescales of magma recharge of large silicic systems from Ti diffusion in quartz. Journal of Petrology, 53, 1385–1416.

Morgan, D.J. and Blake, S. (2006) Magmatic residence times of zoned phenocrysts: introduction and application of the binary element diffusion modeling (BEDM) technique. Contributions to Mineralogy and Petrology, 151, 58–70.

Pamukcu, A.S., Ghiorso, M.S., Gualda, G.A. (2016) High-Ti, bright-CL rims in volcanic quartz: a result of very rapid growth. Contributions to Mineralogy and Petrology 172, 9pp.

Peppard, B.T, Steele, I.M., Davis, A.M., Wallace, P.J., Anderson, A.T. (2001) Zoned quartz phenocrysts from the rhyolitic Bishop Tuff. American Mineralogist 86(9), 1034-1052.

Phillips, E.H., Goff, F., Kyle, P.R., McIntosh, W.C., Dunbar, N.W., and Gardner, J.N. (2007) The $^{40}Ar/^{39}Ar$ age contraints on the duration of resurgence at the Valles caldera, New Mexico. Journal of Geophysical Research, 112, B08201, 15 p.

Reid, M.R. and Vasquez, J.A. (2017) Fitful and protracted assembly leading to a giant eruption, Youngest Toba Tuff, Indonesia. Geochemistry, Geophysics, Geosystems 18, 156–177.

Seitz, S., Putlitz, B., Baumgartner, L.P., Escrig, S., Meibom, A., and Bouvier, A.-S. (2016) Short magmatic residence times of quartz phenocrysts in Patagonian rhyolites associate dwith Gondwana breakup. Geology, 44, 67–70.

Self, S., Goff, F., Gardner, J.N., Wright, J.V. and Kite, W. (1986) Explosive rhyolitic volcanism in the Jemez Mountains: Vent locations, caldera development and relation to regional structure. Journal of Geophysical Research, 91, 1779–1798.

Always consult and cite the final, published document. See http:/www.minsocam.org or GeoscienceWorld

This is the peer-reviewed, final accepted version for American Mineralogist, published by the Mineralogical Society of America.
The published version is subject to change. Cite as Authors (Year) Title. American Mineralogist, in press.
DOI: https://doi.org/10.2138/am-2020-7395. http://www.minsocam.org/

Self, S., Heiken, G., Sykes, M.L., Wohletz, K., Fisher, R.V., and Dethier, D.P. (1996) Field excursions to the Jemez Mountains, New Mexico. Bulletin of the New Mexico Bureau of Geology and Mineral Resources, 134, 72 pp.

Shane, P., Smith, V.C., Narin, I. (2008) Millennial timescale resolution of rhyolite magma recharge at Tarawera volcano: insights from quartz chemistry and melt inclusions. Contributions to Mineralogy and Petrology 156, 397-411.

Shea, T., Costa, F., Krimer, D., and Hammer, J.E. (2015) Accuracy of timescales retrieved from diffusion modeling in olivine: a 3D perspective. American Mineralogist, 100, 2026–2042.

Simon, J.L. and Reid, M.R. (2005) The pace of rhyolite differentiation and storage in an 'archetypa' silicic magma system, Long Valley, California. Earth and Planetary Science Letters, 235, 123–140.

Smith, R.L. and Bailey, R.A. (1966) The Bandelier Tuff - a study of ash-flow eruption cycles from zoned magma chambers. Bulletin Volcanologique, 29, 83–104.

Stimac, J.A. (1996) Hornblende-dacite pumice in the Tshirege member of the the Bandelier Tuff: Implications for magma chamber and eruptive processes. New Mexico Geological Society, 47th Field Conference Guidebook, 269–274.

Thomas, J.B. and Watson, E.B. (2012) Application of the Ti-in-quartz thermobarometer to rutile-free systems. Reply to: a comment on: 'TitaniQ under pressure: the effect of pressure and temperature on the solubility of Ti in quartz' by Thomas et al. Contributions to Mineralogy and Petrology, 164, 369–374.

Thomas, J.B., Watson, E.B., Spear, F.S., Shemella, P.T., Nayak, S.K., and Lanzirotti, A. (2010) TitaniQ under pressure: the effect of pressure and temperature on the solubility of Ti in quartz. Contributions to Mineralogy and Petrology, 160, 743–759.

Till, C.B., Vasqez, J.A. and Boyce, J.W. (2015) Months between rejuvenation and volcanic eruption at Yellowstone caldera, Wyoming. Geology, 43, 695–698.

Torres, R.C., Self, S. and Martinez, M.M.L. (1996) Secondary pyroclastic flows from the June 15, 1991, ignimbrite of Mount Pinatubo. In C.G. Newhall, R.S. Punongbayan, eds., Fire and Mud: eruptions and lahars of Mount Pinatubo, Philippines. Philippine Institute of Volcanology and Seismology and University of Washington Press, pp. 665–678.

Trial, A.F., Spera, F.J., Greer, J. and Yuen, D.A. (1992) Simulations of magma withdrawal from compositionally zoned bodies. Journal of Geophysical Research, 97, 6713–6733.

Always consult and cite the final, published document. See http:/www.minsocam.org or GeoscienceWorld

This is the peer-reviewed, final accepted version for American Mineralogist, published by the Mineralogical Society of America.
The published version is subject to change. Cite as Authors (Year) Title. American Mineralogist, in press.
DOI: https://doi.org/10.2138/am-2020-7395. http://www.minsocam.org/

Tuttle, O.F. and Bowen, N.L. (1958) Origin of granite in the light of experimental studies in the system $NaAlSi_3O_8$-$KAlSi_3O_8$-SiO_2-H_2O. Geological Society of America Memoir, 74, 153 pp.

Wark, D.A. and Watson, E.B. (2006) TitaniQ: a titanium-in-quartz geothermometer. Contributions to Mineralogy and Petrology, 152, 743–754.

Wark, D.A., Hildreth, W., Spear, F.S., Cherniak, D.J., and Watson, E.B. (2007) Pre-eruption recharge of the Bishop magma system. Geology, 35, 235–238.

Warren, R.G., Goff, F., Kluk, E.C., and Budahn, J.R. (2007) Petrography, chemistry, and mineral compositions for subunits of the Tshirege Member, Bandelier Tuff, within the Valles caldera and Pajarito Plateau: New Mexico Geological Society, 58th Field Conference Guidebook, 316–332.

Warshaw, C.M. and Smith, R.L. (1988) Pyroxenes and fayalites in the Bandelier Tuff, New Mexico: temperatures and comparison with other rhyolites. American Mineralogist, 73, 1025–1037.

Wilcock, J., Goff, F., Minarik, W.G., and Stix, J. (2013) Magmatic rewcharge during the formation and resurgence of the Valles calderam New Mexico, USA: evidence from quartz compositional zoning and geothermometry. Journal of Petrology, 54, 635–664.

Wilson, C.J.N., Seward, T.M., Allan, A.S.R., Charlier, B.L.A. and Bello, L. (2012) A comment on: 'TitaniQ under pressure: the effect of pressure and temperature on the siolubility of Ti in quartz', by Jay B. Thomas, E. Bruce Watson, Frank S. Spear, Philip Shemella, Saroj K. Nayak and Antonio Lanzirotti. Contributions to Mineralogy and Petrology, 164, 359–368.

Wolff, J.A. and Ramos, F.C. (2014) Processes in caldera-forming high-silica rhyolite magma: Rb-Sr and Pb isotope systematics of the Otowi Member of the Bandelier Tuff, Valles Caldera, New Mexico, USA. Journal of Petrology, 55, 345–375.

Wolff, J.A., Ellis, B.S., Ramos, F.C., Starkel, W.A., Boroughs, S., Olin, P.H. and Bachmann, O. (2015) Remelting of cumulates as a process for producing chemical zoing in silicic tuffs: a comparison of cool, wet and hot, dry rhyolitic magma systems. Lithos, 236–237, 275–286.

Wolff, J.A., Forni, F., Ellis, B.S. and Szymanowski, D. (2020) Europium and barium enrichments in compostionally zoned felsic tuffs: A smoking gun for the origin of chemical and physical gradients by cumulate melting. Earth and Planetary Science Letters 540:116251, 12 pp.

Always consult and cite the final, published document. See http:/www.minsocam.org or GeoscienceWorld

This is the peer-reviewed, final accepted version for American Mineralogist, published by the Mineralogical Society of America.
The published version is subject to change. Cite as Authors (Year) Title. American Mineralogist, in press.
DOI: https://doi.org/10.2138/am-2020-7395. http://www.minsocam.org/

FIGURE CAPTIONS

FIGURE 1. Cathodoluminescence grayscale images of representative quartz crystals from four different samples of the Tshirege Member, Bandelier Tuff, arranged in stratigraphic order. Note increasing complexity of CL-zoning upwards through the Tshirege Member. Crystallized melt inclusions appear bright; glassy inclusions are near-black.

FIGURE 2. Concentrations of Th and Nb in whole pumices plotted for the Tshirege Member. Notice the bimodal distribution of the high-silica rhyolite magmas, allowing distinction of three magma types (enriched high-silica rhyolite, HSR-e; depleted high-silica rhyolite HSR-d, and low-silica rhyolite, LSR; see also Table 4).

FIGURE 3. Trace element variations among Tshirege glasses; EG = external glass, MI = melt inclusion. **a.** Th vs. Nb; **b.** La vs. Hf; **c.** Hf/La vs Rb. **d.** Rb/Sr vs Ba/La, with faceted inclusions identified – see text.

FIGURE 4. **a.** Faceting strength (FS) vs Ba concentration; explanation of FS given in text. **b.** Crystal containing melt inclusions with FS = 0 and 0.5. **c.** FS = 1 and 1.5. **d.** FS = 2. Note that not all crystals exhibit all FS values. **e.** Sketch comparison of FS categories and qualifications for any given FS value.

FIGURE 5. Back-scatter electron image of a quartz crystal from HSR-d pumice hosting four melt inclusions (light gray). White numbers indicate FS rating; each inclusion is labeled with Ba and Sr concentrations. Gray dashed line shows interpreted original crystal boundary, before regrowth event. Note elevated Ba and Sr in the low FS inclusions in the interpreted rim. This crystal has no CL zoning.

Always consult and cite the final, published document. See http:/www.minsocam.org or GeoscienceWorld

This is the peer-reviewed, final accepted version for American Mineralogist, published by the Mineralogical Society of America.
The published version is subject to change. Cite as Authors (Year) Title. American Mineralogist, in press.
DOI: https://doi.org/10.2138/am-2020-7395. http://www.minsocam.org/

819 **FIGURE 6.** Titanium concentration and CL grayscale intensity profiles of four representative
820 quartz crystals from the Tshirege (158-3, 88-1, 151-3, and 90-1) with modeled diffusion curves
821 ([Ti]: solid black lines; CL: dashed grey lines), calculated from eqns. (4) – (6). Error bars for [Ti]
822 points are smaller than symbol size. Transect data are cropped to the diffusional relaxation zone;
823 full transects can be found in supplementary data. CL grayscale images and transect locations are
824 included for each sample *OC = oblique corrected transect; explanation in supplementary data
825 file. C = diffusion times calculated using D_{Ti} from Cherniak et al. (2007); J = diffusion times
826 calculated using D_{Ti} from Jollands et al. (2020).

827

828 **FIGURE 7.** A simplified four stage model showing the development of the CL zoning and melt
829 inclusion chemistry for the Tshirege magmas. **a.** Initial stage: accumulation of crystals, some
830 with melt inclusions depleted in compatible trace elements. **b.** Mature high-crystallinity mush;
831 ongoing faceting of melt inclusions on a ~1,000-10,000 year timescale. **c.** More primitive
832 magma starts to recharge the system with heating and possible release of volatiles, causing
833 resorption of quartz and feldspar. **d.** Quartz grows at higher temperatures trapping melt
834 inclusions with higher concentrations of compatible trace elements (i.e., Ba and Sr). Eventually,
835 the system overpressurizes to the point of eruption.

836

837 **TABLES**

838 **Table 1.** LA-ICP-MS and EPMA data for selected samples.

839 **Table 2.** Data from diffusion modeling results and titanium in quartz thermometry results using
840 D_{Ti} from Cherniak et al. (2007) "Nb (ppm)" is the concentration of Nb in the host pumice.

Always consult and cite the final, published document. See http:/www.minsocam.org or GeoscienceWorld

This is the peer-reviewed, final accepted version for American Mineralogist, published by the Mineralogical Society of America.
The published version is subject to change. Cite as Authors (Year) Title. American Mineralogist, in press.
DOI: https://doi.org/10.2138/am-2020-7395. http://www.minsocam.org/

841 **Table 3.** Data from diffusion modeling results and titanium in quartz thermometry results using
842 D_{Ti} from Jollands et al. (2020).

843 **Table 4.** XRF analyses of whole pumice clasts from which quartz crystals were sampled and
844 analyzed (Table 2). Sample 9 is from the Tsankawi Pumice and quartz-glass data from this
845 sample were used to calibrate a_{TiO_2} for TitaniQ.

Always consult and cite the final, published document. See http:/www.minsocam.org or GeoscienceWorld

This is the peer-reviewed, final accepted version for American Mineralogist, published by the Mineralogical Society of America.
The published version is subject to change. Cite as Authors (Year) Title. American Mineralogist, in press.
DOI: https://doi.org/10.2138/am-2020-7395. http://www.minsocam.org/

Table 1: LA-ICPMS vs WDS-EMPA for [Ti] in quartz

Sample:	LA-ICPMS (ppm)	WDS average (ppm)
Cores:		
158-3	26.8 ± 1.3	24.7 ± 1.5
151-1	28.7 ± 2.5	29.5 ± 1.0
104-5	30.8 ± 2.4	32.7 ± 1.1
151-3	35.8 ± 2.8	34.5 ± 0.9
Rims:		
158-3	44.4 ± 2.2	42.4 ± 1.1
151-1	44.7 ± 3.1	48.4 ± 0.7
104-5	48.2 ± 2.8	51.1 ± 1.7
151-3	45.7 ± 3.6	46.3 ± 1.3

Errors reported in 1σ

Always consult and cite the final, published document. See http:/www.minsocam.org or GeoscienceWorld

This is the peer-reviewed, final accepted version for American Mineralogist, published by the Mineralogical Society of America.
The published version is subject to change. Cite as Authors (Year) Title. American Mineralogist, in press.
DOI: https://doi.org/10.2138/am-2020-7395. http://www.minsocam.org/

Table 2: Diffusion Modeling Results

Sample	CL Model time			[Ti] model time			Model times $a(TiO_2)$			Model times $\gamma(TiO_2)$			Nb
Tshirege	time (years)	error[a]		time (years)	error[a]		time (years)	error[b]	*T* used (°C)	time (years)	error[b]	*T* used (°C)	(ppm)
88-1	2060	+824	-1236	10400	+4160	-6000	980	± 95	825	2200	± 275	799	37
151-3[c]	520	+208	-312	<520	+208	-312	<525	± 90	748	<780	± 140	727	64
151-1[c]	300	+120	-180	920	+368	-552	930	± 180	748	2300	±300	727	64
104-4-2	180	+72	-108	240	+96	-144	<155	± 60	778	<490	± 220	731	65
104-5-1	160	+64	-96	<190	+76	-114	<185	± 80	752	<780	± 600	703	65
104-5-2	—	—	—	<270	+108	-162	<265	± 120	752	<900	± 600	703	65
141-1-1	400	+160	-240	2000	+800	-1200	1150	± 250	786	2000	± 550	748	68
141-2-1	—	—	—	<400	+160	-240	<150	± 60	786	<300	± 100	758	68
141-2-2	120	+48	-72	<180	+72	-108	<90	± 60	786	<160	± 90	758	68
119-3	600	+240	-360	900	+360	-560	250	±40	783	480	± 90	762	69
119-4-OC	—	—	—	150	+60	-90	60	±15	783	105	± 20	762	69
158-3	120	+48	-72	1200	+480	-180	610	± 120	778	2300	± 300	724	68
90-1	55	+22	-33	<280	+120	-45	<140	± 40	773	<265	± 55	753	73
90-1-OC	—	—	—	210	+88	-132	115	± 20	773	170	± 25	753	73
90-3	100	+40	-60	<1100	+440	-660	<650	± 105	783	<1050	± 215	753	73
90-3-OC	—	—	—	180	+72	-108	150	± 20	783	175	± 15	753	73
90-4	640	+248	-372	800	+96	-36	410	± 75	775	980	± 115	742	73

First two columns are calculated using 750°C to allow for comparison of the two profiles.
[a]Errors arising from the error on the diffusion coefficient (Cherniak et al., 2007), calculated at a fixed *T* = 750 °C.
[b]Errors from fitting diffusion sigmoid to data; errors from uncertainty of diffusion coefficient not included.
[c]No glass Ti contents measured; average Tshirege glass Ti concentration used for temperature estimation.
OC = oblique corrected transect. See supplemental data for explanation of oblique correction

This is the peer-reviewed, final accepted version for American Mineralogist, published by the Mineralogical Society of America.
The published version is subject to change. Cite as Authors (Year) Title. American Mineralogist, in press.
DOI: https://doi.org/10.2138/am-2020-7395. http://www.minsocam.org/

Table 3: Diffusion modeling results

Sample	Model times $a(TiO_2)$				Model times $\gamma(TiO_2)$			
	Model Time (years)		error	*T* used (°C)	Model Time (years)		error	*T* used (°C)
88-1	1.1E+06	±	9.9E+03	825	5.65E+06	±	8.5E+04	799
151-3	<3.1E+05	±	9.9E+03	748	<6.95E+05	±	2.2E+04	727
151-1	9.9E+05	±	8.9E+03	748	6.18E+06	±	1.0E+05	727
104-4-2	<2.66E+04	±	3.6E+04	778	<2.72E+05	±	5.4E+04	731
104-5-1	<3.80E+04	±	3.9E+03	752	6.95E+05	±	4.1E+05	703
104-5-2	<7.85E+04	±	7.0E+03	752	<9.28E+05	±	4.1E+05	703
141-1-1	1.52E+06	±	1.6E+04	786	4.66E+06	±	3.4E+05	748
141-2-1	<2.49E+04	±	7.0E+04	786	<1.01E+05	±	1.1E+04	758
141-2-2	<8.86E+03	±	3.9E+03	786	<2.83E+04	±	8.9E+03	758
119-3	6.98E+04	±	3.9E+03	783	2.61E+05	±	8.9E+03	762
119-4-OC	3.91E+03	±	7.3E+02	783	1.21E+04	±	4.2E+02	762
158-3	4.23E+05	±	2.4E+02	778	6.18E+06	±	1.0E+05	724
90-1	<2.16E+04	±	1.6E+04	773	<7.85E+04	±	3.3E+03	753
90-1-OC	1.45E+04	±	1.7E+03	773	3.20E+04	±	6.7E+02	753
90-3	<4.81E+05	±	4.2E+02	783	<1.27E+06	±	1.0E+05	753
90-3-OC	2.48E+05	±	2.2E+03	783	3.40E+05	±	2.4E+02	753
90-4	1.90E+05	±	4.2E+02	775	1.10E+06	±	2.4E+02	742

Diffusional relaxation times calculated using D_{Ti} of Jollands et al. (2020).
Errors listed are from fitting of the diffusion sigmoid to data.

This is the peer-reviewed, final accepted version for American Mineralogist, published by the Mineralogical Society of America.
The published version is subject to change. Cite as Authors (Year) Title. American Mineralogist, in press.
DOI: https://doi.org/10.2138/am-2020-7395. http://www.minsocam.org/

Table 4: Whole Pumice Analyses

Major and minor elements (wt%)								
Sample	**88**	**90**	**104**	**119**	**141**	**151**	**158**	**9**
SiO_2	69.58	78.57	74.69	78.44	78.96	79.07	79.82	75.70
TiO_2	0.42	0.08	0.08	0.07	0.08	0.07	0.09	0.09
Al_2O_3	15.87	12.21	11.83	11.70	11.40	11.45	11.44	13.53
FeO*	3.30	1.36	1.33	1.19	1.26	1.18	1.38	1.85
MnO	0.06	0.05	0.04	0.05	0.05	0.05	0.05	0.09
MgO	0.98	0.01	0.15	0.13	0.05	0.16	0.02	0.11
CaO	2.44	0.37	1.23	0.77	0.41	0.70	0.26	0.36
Na_2O	3.59	2.67	3.18	2.90	2.96	2.87	2.58	3.07
K_2O	3.64	4.67	7.43	4.71	4.82	4.43	4.34	5.18
P_2O_5	0.13	0.01	0.03	0.04	0.02	0.03	0.02	0.02
Trace elements (ppm)								
Zn	109	77	74	74	73	76	72	152
Ga	24	24	21	22	22	22	22	29
Rb	112	158	133	151	147	142	144	273
Sr	323	9	40	19	21	28	7	30
Y	53	72	91	65	70	60	58	183
Zr	268	213	198	204	213	199	223	289
Nb	37	73	65	69	68	64	68	153
Ba	559	93	70	67	49	52	52	64
La	63	69	62	61	69	63	62	67
Ce	101	118	112	112	117	118	118	120
Nd	46	53	53	49	49	48	45	54
Pb	463	43	111	28	50	38	92	63
Th	15	22	20	22	21	20	22	38

[a]FeO = Fe_{Total}

Major oxides normalized to a volatile-free basis

Always consult and cite the final, published document. See http:/www.minsocam.org or GeoscienceWorld

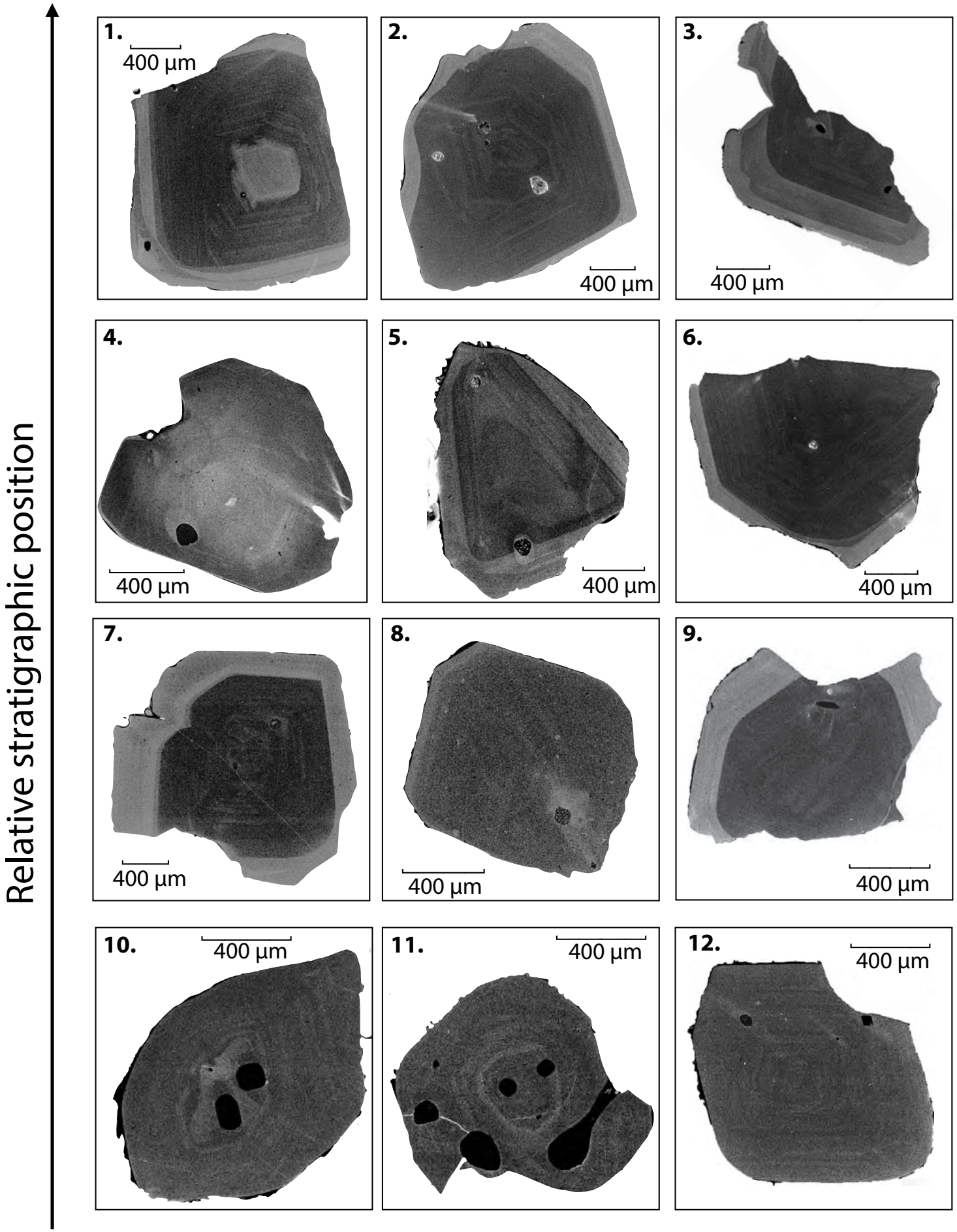
Relative stratigraphic position
1.
400 µm
2.
400 µm
3.
400 µm
4.
400 µm
5.
400 µm
6.
400 µm
7.
400 µm
8.
400 µm
9.
400 µm
10.
400 µm
11.
400 µm
12.
400 µm

Figure 1

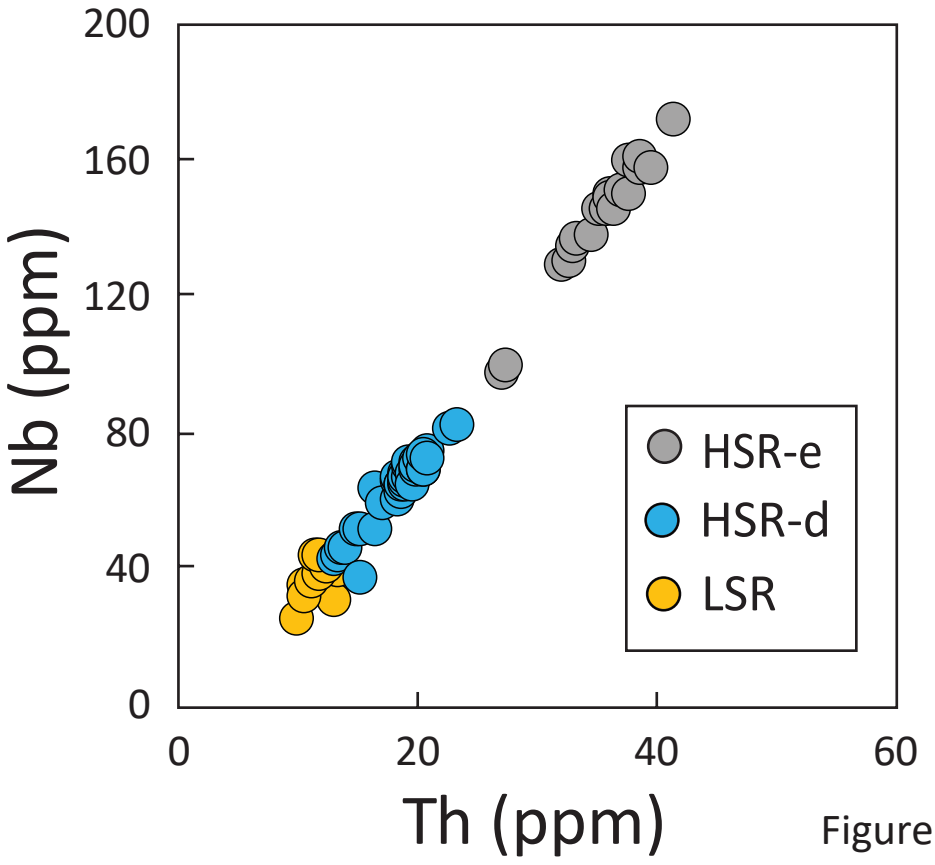

Figure 2

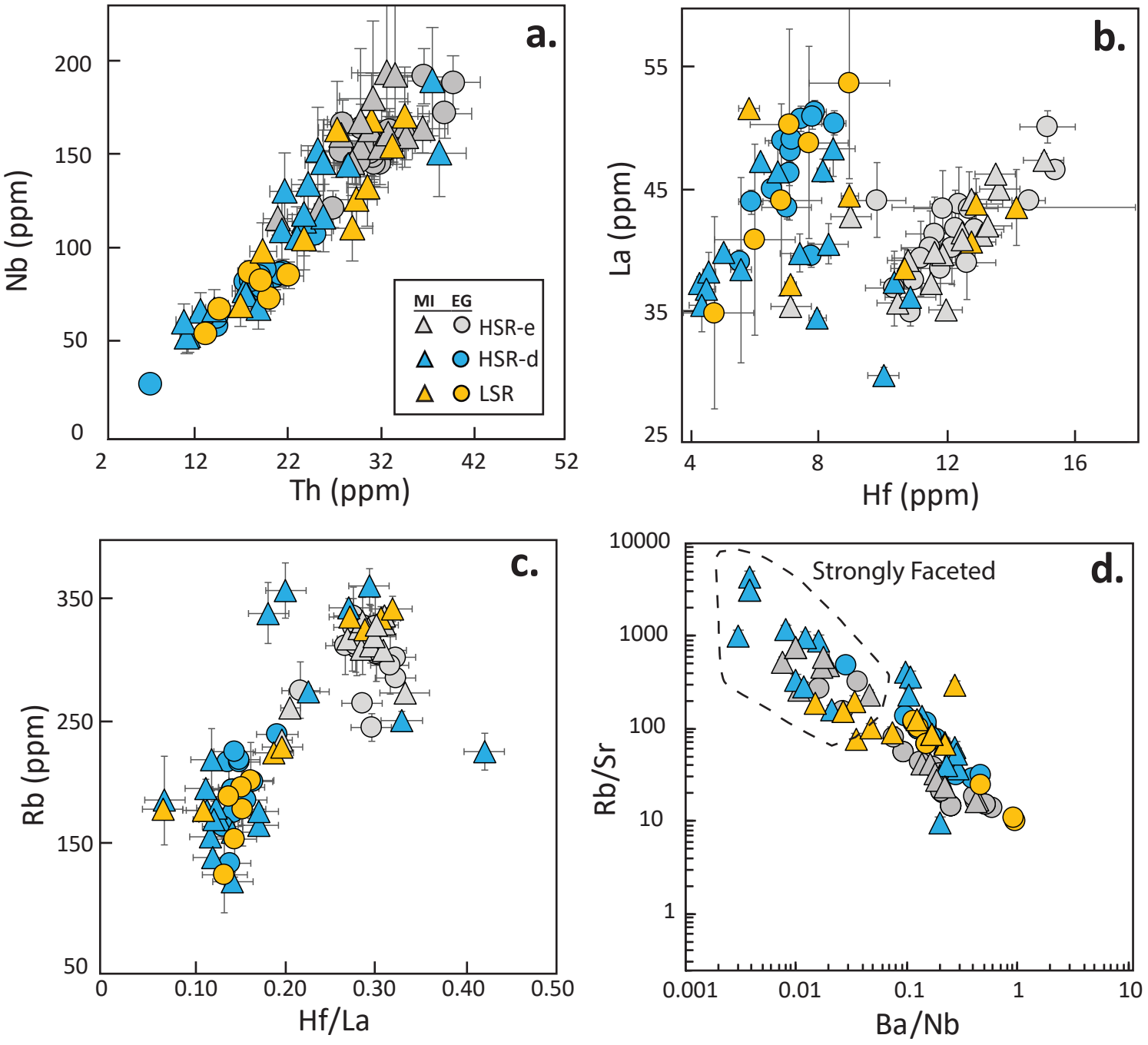
a.
Nb (ppm)
Th (ppm)
MI EG
HSR-e
HSR-d
LSR
b.
La (ppm)
Hf (ppm)
c.
Rb (ppm)
Hf/La
d.
Strongly Faceted
Rb/Sr
Ba/Nb

Figure 3

Figure 4

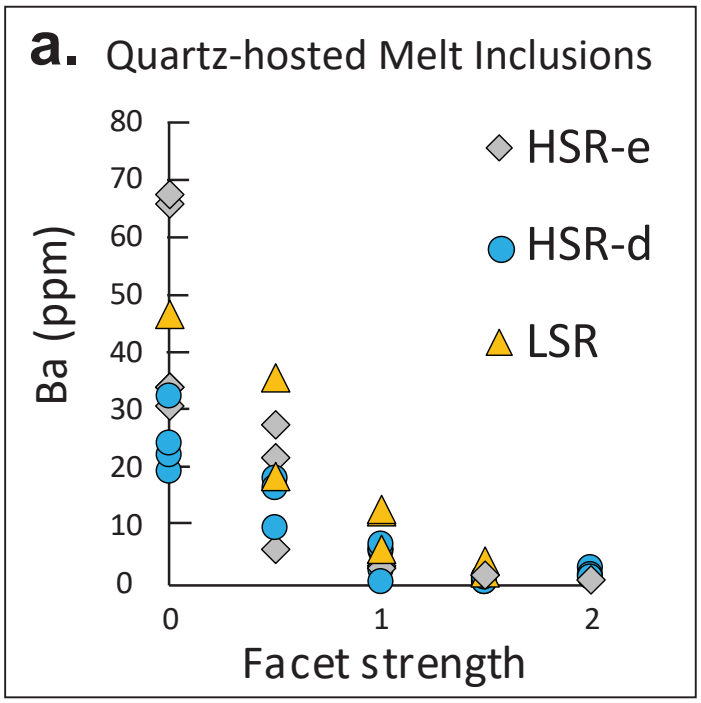
a.
Quartz-hosted Melt Inclusions
Ba (ppm)
80
70
60
50
40
30
20
10
0
0
1
2
Facet strength
HSR-e
HSR-d
LSR

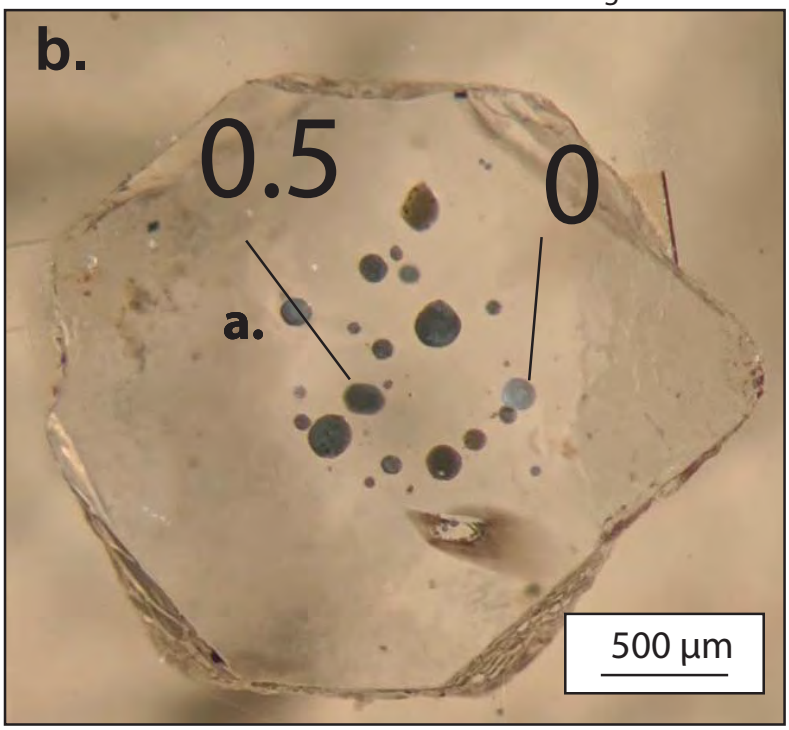
b.
0.5
0
a.
500 µm

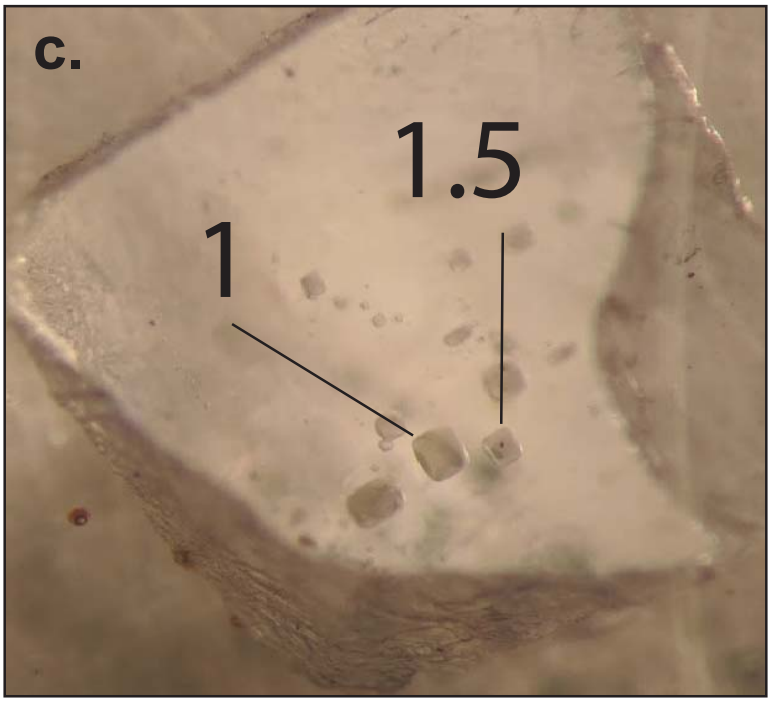
c.
1.5
1

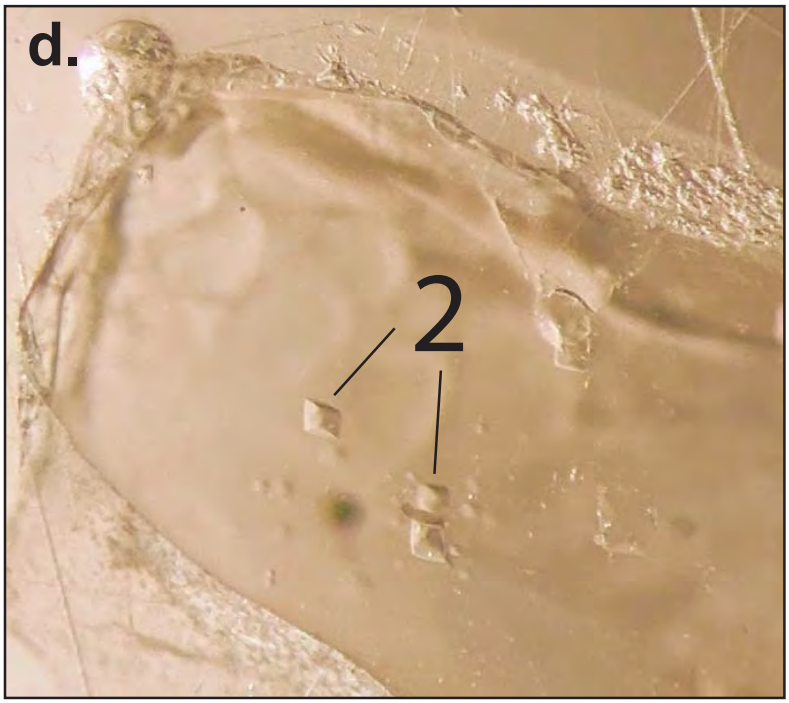
d.
2

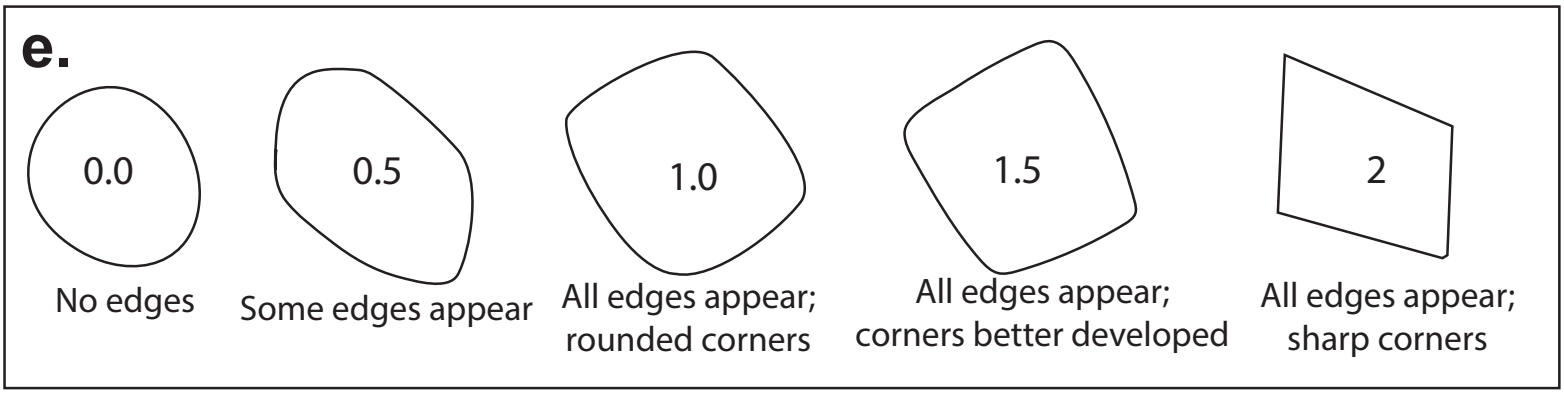
e.
0.0
No edges
0.5
Some edges appear
1.0
All edges appear; rounded corners
1.5
All edges appear; corners better developed
2
All edges appear; sharp corners

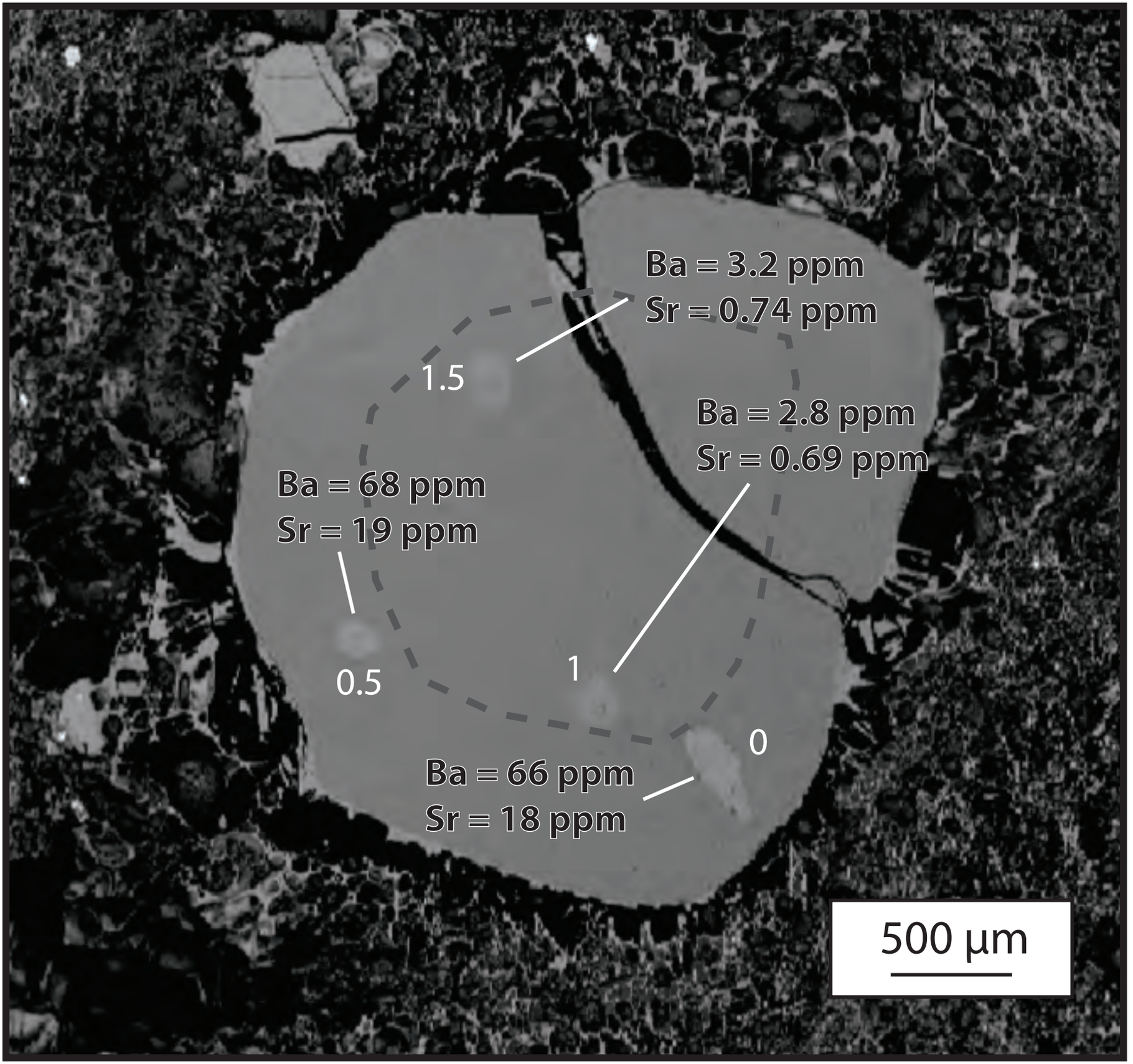
Ba = 3.2 ppm
Sr = 0.74 ppm
1.5
Ba = 2.8 ppm
Sr = 0.69 ppm
Ba = 68 ppm
Sr = 19 ppm
0.5
1
0
Ba = 66 ppm
Sr = 18 ppm
500 µm

Figure 5

Figure 6

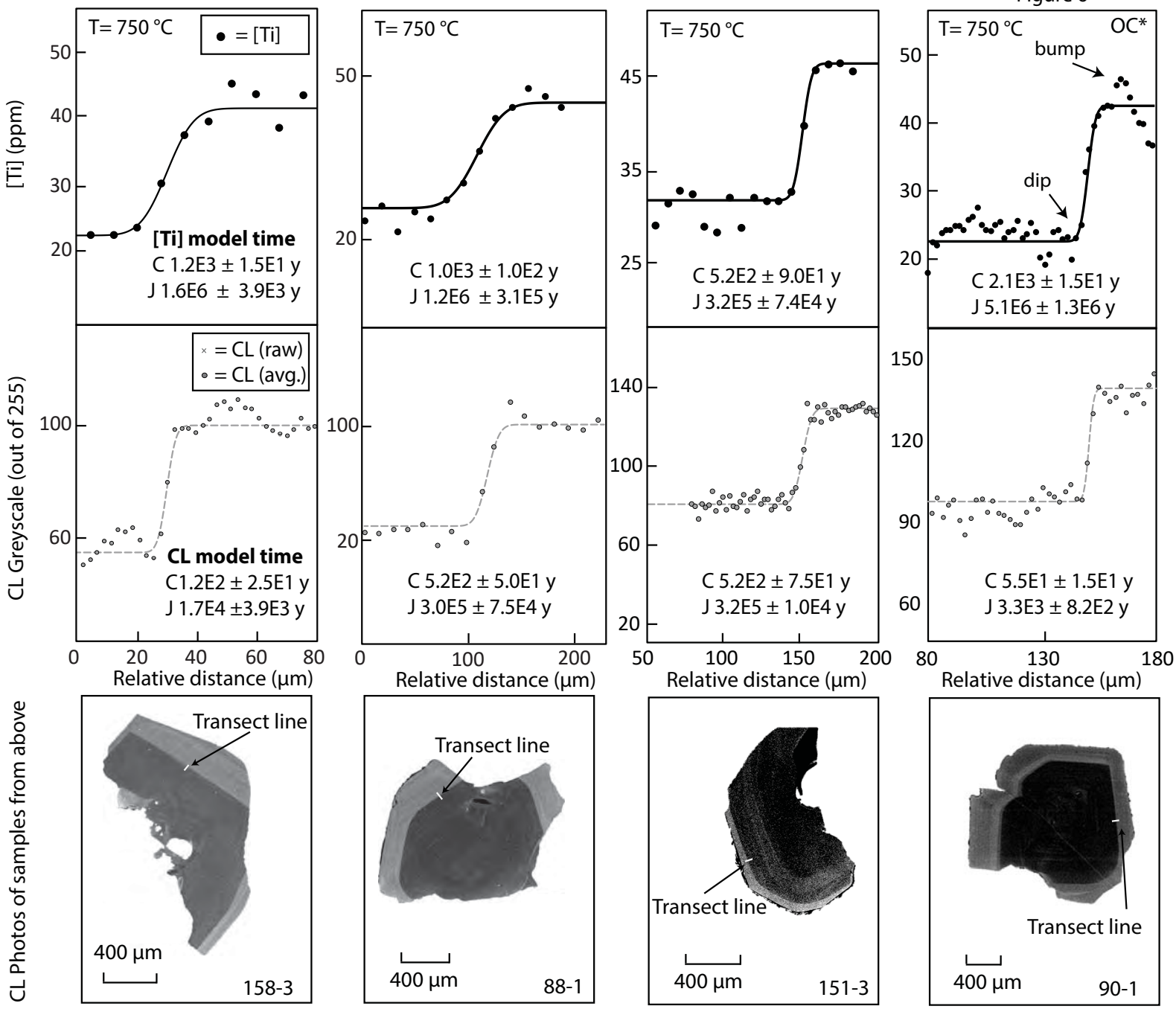
T= 750 °C
= [Ti]
[Ti] (ppm)
[Ti] model time
C 1.2E3 ± 1.5E1 y
J 1.6E6 ± 3.9E3 y
T= 750 °C
C 1.0E3 ± 1.0E2 y
J 1.2E6 ± 3.1E5 y
T= 750 °C
C 5.2E2 ± 9.0E1 y
J 3.2E5 ± 7.4E4 y
T= 750 °C
OC*
bump
dip
C 2.1E3 ± 1.5E1 y
J 5.1E6 ± 1.3E6 y
= CL (raw)
= CL (avg.)
CL Greyscale (out of 255)
CL model time
C1.2E2 ± 2.5E1 y
J 1.7E4 ±3.9E3 y
C 5.2E2 ± 5.0E1 y
J 3.0E5 ± 7.5E4 y
C 5.2E2 ± 7.5E1 y
J 3.2E5 ± 1.0E4 y
C 5.5E1 ± 1.5E1 y
J 3.3E3 ± 8.2E2 y
Relative distance (µm)
Relative distance (µm)
Relative distance (µm)
Relative distance (µm)
CL Photos of samples from above
Transect line
400 µm
158-3
Transect line
400 µm
88-1
Transect line
400 µm
151-3
Transect line
400 µm
90-1

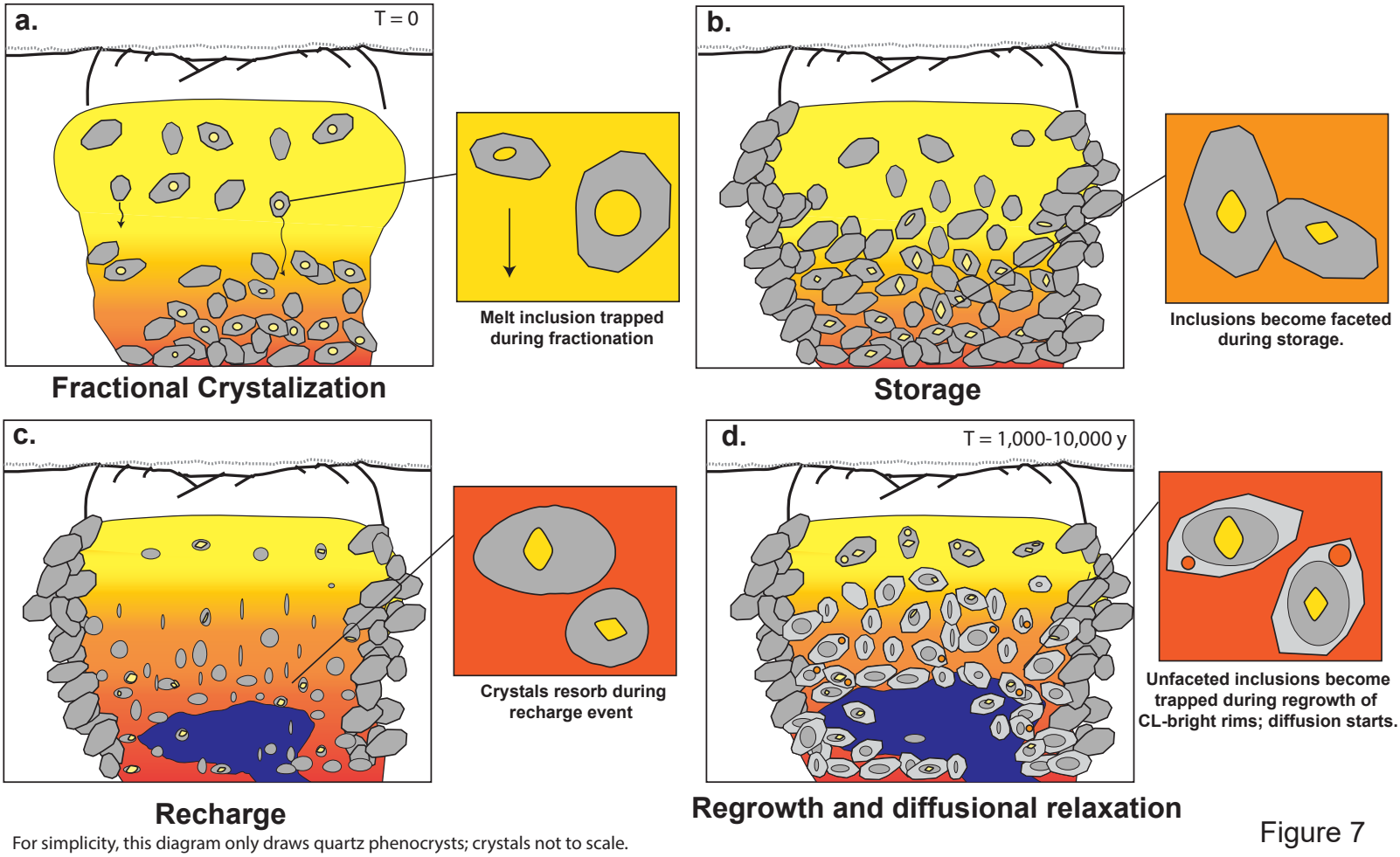

For simplicity, this diagram only draws quartz phenocrysts; crystals not to scale.

Figure 7